frontiers | Frontiers in Earth Science

TYPE Original Research
PUBLISHED 11 October 2023
DOI 10.3389/feart.2023.1260852

OPEN ACCESS

EDITED BY
Huan Li,
Central South University, China

REVIEWED BY
Liang Qiu,
China University of Geosciences, China
Fei Wu,
China University of Geosciences Wuhan, China
Hossein Azizi,
University of Kurdistan, Iran

*CORRESPONDENCE
Chao Chen,
chen_cug@foxmail.com

RECEIVED 18 July 2023
ACCEPTED 21 September 2023
PUBLISHED 11 October 2023

CITATION
Liu R, Chen C, Lv X, Zhang Z, Ruan B, Zhang S and Hu E (2023), Petrogenesis and geological implications of the qiyishan triassic granitoids in east Beishan orogen, inner Mongolia, NW China: evidence from geochronology, geochemistry and Nd-Hf isotopes. *Front. Earth Sci.* 11:1260852. doi: 10.3389/feart.2023.1260852

Petrogenesis and geological implications of the qiyishan triassic granitoids in east Beishan orogen, inner Mongolia, NW China: evidence from geochronology, geochemistry and Nd-Hf isotopes

Ruiqin Liu[1], Chao Chen[2]*, Xinbiao Lv[1], Zhongcheng Zhang[1], Banxiao Ruan[2], Shanming Zhang[3] and Erhong Hu[4]

[1]Faculty of Earth Resources, China University of Geosciences (Wuhan), Wuhan, China, [2]Institute of Geological Survey, China University of Geoscience Wuhan, Wuhan, China, [3]Faculty of Mining, Inner Mongolia University of Technology, Huhehaote, China, [4]Inner Mongolia Yunfan Geological Environment Technical Service Co LTD, Wuhai, China

The Qiyishan deposit is a large-scale Rb polymetallic deposit in the Beishan orogen. However, there remain debates regarding its metallogenic age and tectonic setting. In addition, studies of Triassic tectono-magmatic events in the Beishan orogen are still insufficient, and conducting genesis studies on the Qiyishan Triassic granitoids will help to enhance the understanding of Triassic magmatism and tectonic evolution in the Beishan orogen. In this contribution, we report new data for the ore-forming granitoids of Qiyishan deposit, including zircon U-Pb ages, major and trace element concentrations and Nd-Hf isotope compositions to define the ages and genesis of the Qiyishan granitoids and discuss their origin and geodynamic implications. Zircon U-Pb dating of the Qiyishan ore-forming granitoids yielded three ages of 217.5 ± 1.3 Ma, 217.2 ±0.8 Ma, and 207.5 ± 2.0 Ma, respectively. The age of Rb mineralization can be constrained to 207.5± 2.0 Ma, while the age of W-Sn-Mo mineralization is considered to be slightly younger than approximately 217 Ma. The Characteristics of major and trace elements of the rock samples indicate that the Qiyishan granites can be classified to highly fractionated I-type granite, and characterised by a transition to A-type like granite to some extent. The granites were not only affected by fractional crystallisation, but also underwent magmatic-hydrothermal interaction. The zircon εHf(t) values of the Qiyishan granitoids ranged from 3.28 to 16.07 and the Hf model age (TDMc) ranged from 0.216 to 1.042 Ga, revealing that the Qiyishan granitoids originated from the partial melting of both mantle and crustal sources. εNd(t) values ranged from −0.52 to −0.25, with Nd model ages of 0.998 Ga to 1.007 Ga. These results indicate that the granitoids originated from the mantle-derived magmas intruding into the lower crust within an intracontinental extensional environment. Combining the previous studies of Triassic granites in the Beishan orogen and this work, the Triassic granites exhibit a transition from I-type to A-type along the northeast

direction, indicating a decrease in the contribution of ancient crustal to the magma source. We propose that the Qiyishan granitoids formed in a transitional tectonic environment, signifying the shift from post-orogenic to intracontinental extensional settings in beishan orogen during late Triassic.

KEYWORDS

Beishan orogen, Qiyishan pluton, triassic granites, Rb mineralization, tectonic evolution

1 Introduction

The Qiyishan Rb polymetallic deposit is a large-scale rare metal deposit in the Beishan orogen of Inner Mongolia. However, the metallogenic age and tectonic setting of the deposit still remain under debate. Nie et al. (2002) obtained a Sm-Nd isochron age of 511 ± 5 Ma for fluorite and suggested that the mineralisation is related to the upward localisation and crystallographic differentiation of the Caledonian crust mantle-derived granitic magma (Nie et al., 2002a; Nie et al., 2002b; Nie et al., 2002c). Yang et al. (2013) acquired the zircon U-Pb ages of 355-359 Ma from the Qiyishan granite batholith, inferring that the Qiyishan deposit formed during the Late Devonian collisional orogeny. The Rb-Sr isochron age of 128 ± 1 Ma for the Qiyishan alkali granite was obtained by Lv et al. (2011). Their works suggested that Qiyishan granite was formed in the Late Yanshanian period by further differentiation of regional potassic granitic magma in a crustal extrusion-extension environment, and Qiyishan alkali granite is closely related to rare metal mineralisation. Being a representative large-scale rare metal deposit in the Beishan orogen, the determination of its metallogenic age and tectonic setting is crucial for accurately understanding the genesis of the deposit.

The Beishan orogen is an important part of the Central Asian orogenic belt, attracting significant attention from geologists due to its diverse tectonic units, such as micro-land masses, island arcs, residual ocean crust, and accretion mixed rocks (Wu et al., 2021a). Considerable research efforts have been dedicated to study the Palaeozoic orogeny, uncovering a substantial number of synorogenic granitoids and providing insights into the development of Early to Mid-Palaeozoic arcs in various regions of the Palaeo-Asian Ocean. However, compared with the extensive studies of Paleozoic magmatic and tectonic evolution, the researches on Triassic tectono-magmatic events in the Beishan orogen are limited. Only Li et al. (2012), Liu et al. (2006) and others reported on a small number of Triassic plutons located in the Huaniushan-Baishantang arc and the Queershan arc (Liu et al., 2006; Li et al., 2012a). This scarcity of research hinders a comprehensive understanding of regional Triassic magmatic and tectonic evolution, while the study of Qiyishan Triassic granitoids will contribute to the researches on this issue.

Based on detailed field investigation and sampling, in this contribution, we report new data for the ore-forming granitic rocks of Qiyishan Rb polymetallic deposit, including zircon U-Pb isotope ages, major and trace element concentrations and Nd-Hf isotope compositions, and comprehensively define the ages and genesis of the Qiyishan granitic rocks and discuss its origin and geodynamic implications. Combining the previous studies of Triassic granites in the Beishan orogen and this work, further discussion is conducted on the regional Triassic magmatic and tectonic evolution in the Beishan region to deepen the understanding of Triassic crustal accretion in this area.

2 Samples and methods

2.1 Regional geological setting

The Beishan orogenic belt is situated in the southwestern region of the Central Asian Orogenic Belt (CAOB). It is demarcated by the East Tianshan orogenic belt to the west, marked by the Xingxingxia Fault. To the east, it shares a border with the Xingmeng orogenic belt, while its northern boundary is defined by the southern Mongolian massif. The southern boundary interfaces with the Dunhuang massif (part of the Tarim Craton), which possesses an Archean foundation (Zuo and He, 1990a; Hsü et al., 1992; Xiao et al., 2010b) (Figure 1A).

The Beishan orogen consists of various geological components, including the Precambrian basement, Palaeozoic arcs, accretionary complexes, ophiolitic mélanges, and arc-related basin sediments (Zuo et al., 1990b; Liu and Wang, 1995; Xiao et al., 2004; Xiao et al., 2010a).

Within the orogen described, multiple major faults and collisional zones have been identified, namely, the Liuyuan-Daqishan Fault, Hongliuhe-Niujuanzi-Xichangjing collisional zone, Xingxingxia Fault, Shaquanzi Fault, and Hongshishan-Pengboshan Fault. These faults demarcate the boundaries of the Beishan orogenic belt, effectively partitioning it into distinct regions from south to north: Daqishgan-Zhangfangshan epicontinental rift, Huaniushan-Baishantang arc, Gongpoquan-Qiyishan block, Xingxingxia-Hanshan block, and Queershan arc (Zhang et al., 2005b; Yang et al., 2012) (Figure 1B).

Remarkable geological features are observed within the Daqishan-Zhangfangshan epicontinental rift, characterized by the presence of Carboniferous clastic sediments originating from terrestrial sources and Early Permian marine clastic sediments. The sedimentary deposits in this region consist of turbidites as well as Permian ultramafic-mafic and felsic magmatic rocks. The coexistence of these rock types signifies the presence of a bimodal igneous series, indicative of a post-collisional environment (Su et al., 2011; Zhang et al., 2011).

The Huaniushan–Baishantang arc comprises a varied assortment of rock types, encompassing metamorphic rocks, clastic rocks demonstrating low-grade metamorphism, volcanic formations, as well as low-grade metamorphic rocks, and volcanic–sedimentary rocks that trace their origins to the Late Palaeozoic period (Zuo and He, 1990a; Zuo et al., 1990b; Zhang, 1993; Liu and Wang, 1995; Nie et al., 2002b). The dominant composition of intrusive rocks in this region is primarily felsic. The intrusive rocks occur widely, containing Early to Mid-Palaeozoic granitoids, Late Palaeozoic granitoids, Palaeozoic mafic and ultramafic intrusions and some Triassic mafic dykes and granitoids (Zuo and He, 1990a; Zuo et al., 1990b; Zhao et al., 2007; Mao et al., 2009; Zhang et al., 2010; Mao et al., 2011; Zhang et al., 2011).

The Hongliuhe–Niujuanzi–Xichangjing fault zone represents an extensive and continuous ophiolitic mélangic zone encompassing a

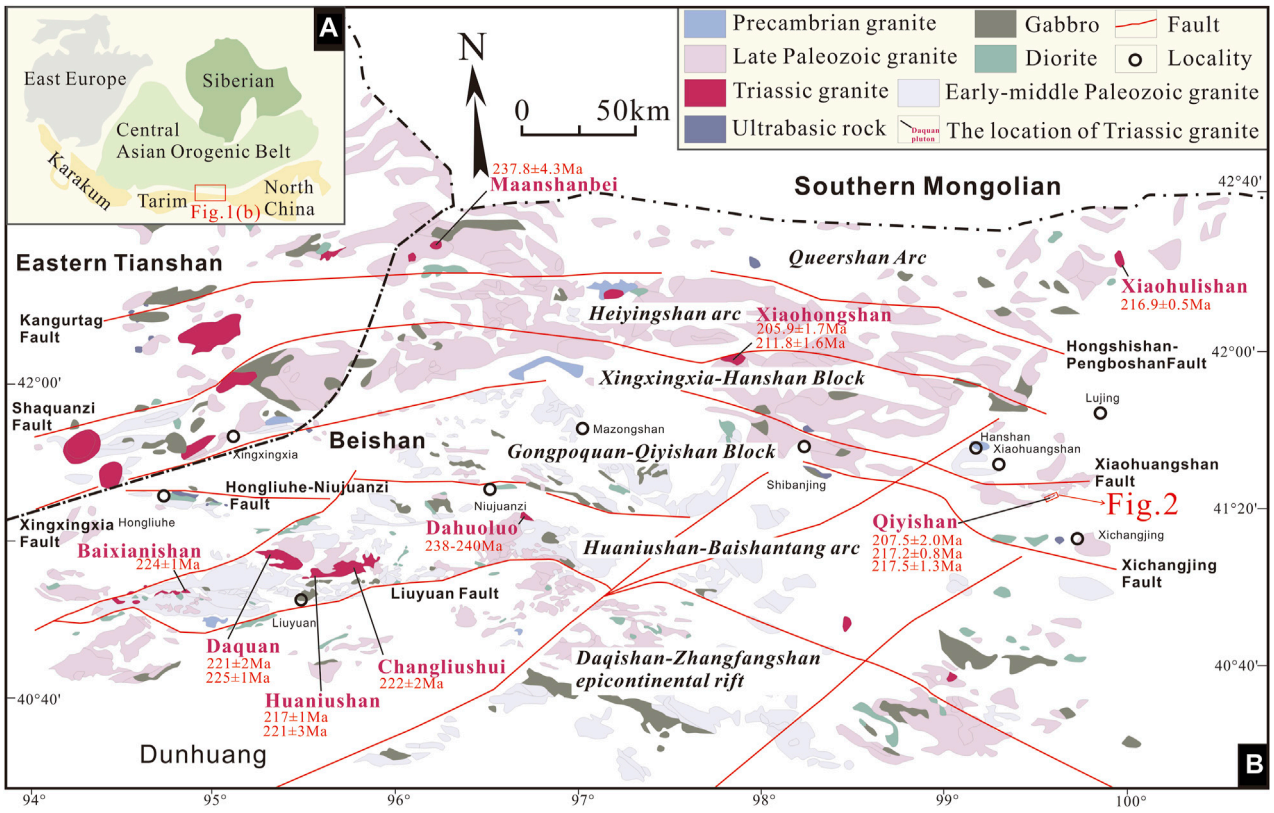

FIGURE 1
(A) The location of the Beishan orogen in the Central Asian Orogenic Belt is depicted in a simplified sketch map (modified from Jahn et al., 2000; Şengör et al., 1993) (Şengör et al., 1993; Jahn et al., 2000). **(B)** A simplified geological map of the Beishan orogen and its surrounding areas displays the Triassic granite plutons' positions (modified based on Li et al., 2009; Li Shan et al., 2012) (Li et al., 2009a; Li et al., 2012b). The ages of the marked granitic plutons were determined using the zircon LA-ICPMS U-Pb method, with age data obtained from various sources, including Li et al., 2006; Li Shan et al., 2012; Li M et al., 2020; Tang et al., 2007; Wang et al., 2010; Zhang Z. Z. et al., 2005; Zhang et al., 2012b; Zhou TF et al., 2010, as well as this article (Zhang et al., 2005b; Li et al., 2006; Tang et al., 2007; Wang et al., 2010; Zhou et al., 2010; Li et al., 2012b; Zhang et al., 2012b; Li et al., 2020).

diverse range of rock types, including clastic rocks, pyroclastic rocks, and ophiolitic rocks (Zuo and He, 1990a; Zuo et al., 1991).

The Gongpoquan–Qiyishan block, also known as the Mazongshan arc, can be subdivided into two distinct parts: the western part and the eastern part. Within the western region, the predominant rock types are characterized by high-grade metamorphic rocks, such as gneisses, schists, and migmatites. Additionally, specific low-grade metamorphic rocks harboring microfossils have been identified, indicative of ages spanning from the Neoproterozoic and Cambrian to the Silurian (Zuo and He, 1990a; Zuo et al., 1991; Liu and Wang, 1995; Mao, 2008). In contrast, the eastern part of the Gongpoquan-Qiyishan block primarily consists of slightly metamorphic volcanic-sedimentary rocks and Late Palaeozoic granites (Zuo and He, 1990a; Zuo et al., 1991). Within the Silurian strata, the Gongpoquan Formation is a noteworthy unit characterized by the occurrence of medium-mafic rocks intermingled with sandstone, da-lite, and siliceous rocks, which are interpreted as remnants of the Palaeozoic arc. Additionally, exposures of Permian sandstones, tuffs, conglomerates, and purple mudstones have been identified (Song et al., 2013).

The Xingxingxia-Shibanjing-Xiaohuangshan fault zone hosts an enduring mélangic zone that stretches in an east-west direction. Within this zone, an assortment of rock types is observed, including meta-ultramafic rocks, mylonitic gabbros, meta-basalts, and clastic rocks, all enveloped within a turbidity matrix (Zuo and He, 1990a; Zuo et al., 1990b; Nie et al., 2002a; Nie et al., 2002b; Nie et al., 2002c; He et al., 2002; He et al., 2005).

The Xingxingxia-Hanshan block is geologically divided by two fault lines: the Xingxingxia-Shibanjing-Xiaohuangshan fault to the south, and the Shaquanzi fault to the north. The Xingxingxia-Hanshan block primarily comprises high-grade metamorphic rocks, although the available age data for the metamorphic events is limited (Liu and Wang, 1995; Xiao et al., 2010a).

The Hongshishan-Pengboshan Fault zone encloses an ophiolitic mélange, where serpentinite predominates as the primary matrix. Within this mélange, a blend of marine sedimentary rocks, including limestones and cherts, coexists with ultramafic and mafic ophiolitic rocks such as pillow basalts and mylonites, which are concentrated in high-strain zones (Zuo and He, 1990a; Zuo et al., 1990b). In contrast, the Heiyingshan arc predominantly consists of Carboniferous felsic volcanic rocks, accompanied by carbonate and clastic sedimentary rocks (Zuo and He, 1990a; Wei et al., 2004; Huang and Jin, 2006).

The Queershan arc exhibits a distinctive assemblage of mafic to intermediate volcanic and volcaniclastic rocks, which originated during

the Ordovician to Permian arcs (Zuo et al., 1991; Zhao et al., 2003; Xiao et al., 2010a). Recent studies have revealed the existence of Triassic granites in this area, such as the Maanshanbei pluton and Xiaohulishan pluton (Liu et al., 2006; Peng et al., 2010; Zhang et al., 2012b). The tectonic evolution of the Beishan orogen is characterized by several distinct stages. The Hongliuhe-Niujuanzi-Xichangjing ocean basin emerged during the Cambrian to Early Silurian period, causing the Dunhuang block and the Queershan arc to separate. This separation is believed to have ended in the Early Devonian. During the Early to Mid-Carboniferous, the Hongshishan-Pengboshan ocean basin formed concurrently with the development of the Huaniushan-Baishantang arc, Mazongshan-Hanshan arc, and Queershan arc (Gong et al., 2002; He et al., 2002; Gong et al., 2003; He et al., 2005; Li et al., 2006; Xiao et al., 2010a). It is widely agreed that these two ocean basins closed no later than the Triassic period, though the exact timing is still disputed. At this stage, the Queershan arc and Heiyingshan arc joined together, and the Xingxingxia-Hanshan block became part of the Huaniushan-Baishantang arc. Transitioning into the Mesozoic-Cenozoic era, the Beishan orogen experienced an intracontinental evolutionary phase (Liu and Wang, 1995; Dumitru and Hendrix, 2001; Gong et al., 2002; Gong et al., 2003; Zuo et al., 2003; Zhang et al., 2005a; Xiao et al., 2010a; Shi et al., 2019).

2.2 Geological setting of the study area

The Qiyishan deposit is located in the eastern section of the Gongpoquan–Qiyishan arc (Figure 1B). It is notable for its Silurian volcanic rocks, which constitute a significant component of the supracrustal sequence, particularly within the Yuanbaoshan and Gongpoquan Formations. Within the formation, there are exposures of metamorphic andesite tuff, while the Gongpoquan Formation can be further subdivided into upper and lower groups. The upper group primarily consists of tuffaceous metamorphic sandstone, whereas the lower group is predominantly composed of andesite marble (Figure 2). The area displays the presence of faults, trending both northwest (NW) and northeast (NE). The Qiyishan Triassic granitic pluton is situated at the intersection of these faults with the NW trend. Spanning an approximate area of 1.3 km^2, the Qiyishan pluton mainly comprises granite and granite porphyry. On the basis of distinctions in location, lithology, mineralization, and alteration, the Qiyishan granitic pluton is segregated into the West Qiyishan Pluton (WQP) and the East Qiyishan Pluton (EQP) by the NS fault (Figure 2). Late Palaeozoic intrusions, such as plagiogranite porphyry and quartz diorite, have also been discovered. The WQP is situated in the western part and intrudes the lower formation of the Gongpoquan tuffaceous metamorphic sandstone and marble. It extends in an east–west direction and is primarily composed of biotite granite, foliaceous biotite granite porphyry, and albitite granitic porphyry. The albitite granitic porphyry is closely linked to rubidium (Rb) mineralization, and a rhomboid Rb ore body has been identified at the center of the pluton. On the other hand, the EQP is positioned in the eastern sector, intruding into the upper formation of Gongpoquan andesite and marble. Geologically extending northeastward, it primarily consists of biotite granite and veined granite porphyry. Notably, the tungsten-tin-molybdenum (W-Sn-Mo) ore body exhibits a significant correlation with the biotite granite, specifically on the eastern side of the EQP (Figure 2).

2.3 Sample descriptions

From the albitite granitic porphyry in the pit that contains the Rb ore body at the center of the West Qiyishan Pluton, we obtained five samples (QY-2, 4, 5, 6, and 7) (Figure 2). The albitite granitic porphyry is characterized by quartz phenocrysts (25%–30%) and albite phenocrysts (20%–25%) embedded in a matrix of muscovite (15%–20%), plagioclase (15%–20%), quartz (15%–20%), kaolinite (5%), and sericite (5%). Accessory minerals, such as zircon and apatite are also present. Plagioclase commonly undergoes sericitization, while albitization is often associated with significant kaolinization (Figures 3A,D,F,H). Additionally, we collected six samples (ZK01021; ZK05045; ZK32031, 2, and 3; and ZK34031) from various bore cores within the East Qiyishan Pluton, which is primarily composed of biotite granite (refer to Figure 2). These samples consist of plagioclase (30%–35%), quartz (25%–30%), biotite (20%–25%), K-feldspar (10%–15%), and muscovite (5%–10%). Plagioclase exhibits approximately 5% sericitization (Figures 3B,C,E,K, l).

2.4 Analytical methods

The following analytical methods were employed in this study: Zircon U-Pb dating and trace element analysis, Major and trace element geochemical analyses, Nd isotopic analyses, and *In-situ* zircon Hf isotopic analyses. Zircons underwent Zircon U-Pb dating and trace element analysis via LAICPMS. For the analysis of major elements in the whole rock, the ZSX Primus II wavelength dispersive Xray fluorescence spectrometer (XRF) manufactured by RIGAKU, Japan, was utilized. The Agilent 7700e ICPMS instrument was employed for trace element analysis of the whole rock. Nd isotopic analyses were conducted using the Neptune Plus MCICPMS instrument by Thermo Fisher Scientific, Dreieich, Germany. *In-situ* zircon Hf isotope ratio analyses were performed using the Neptune Plus MCICPMS instrument. All aforementioned analyses were carried out at Wuhan Sample Solution Analytical Technology Co., Ltd., in Wuhan, China. Supplementary Appendix A provides comprehensive details regarding the analytical methods and experimental conditions utilized.

3 Analytical results

3.1 U–Pb zircon results

The zircon grains from three different granite samples (ZK01021, QY-2, and ZK32031) underwent analysis using LAICPMS. The zircons exhibit euhedral to semi-euhedral shapes, displaying colorless or pale-yellow hues when observed in transmitted light. The particle sizes range from 50 μm to 150 μm, and their length to width ratios fall within the range of 1:1 to 3:1. Cathodoluminescence images reveal oscillating zoning and high Th/U ratios in most of the zircons, indicating their magmatic origin (Figure 4F). For sample ZK01021, eleven concordant points yield a concordia 206 Pb/238U age of 217.5 ± 1.3 Ma (MSWD = 4.8, n = 11), and a weighted mean age of 217.1 ± 1.3 Ma (MSWD = 6.4, n = 11) (Figures 4A,B). Similarly, for sample ZK32031, seventeen concordant points yield a concordia 206 Pb/238U age of 217.2 ±

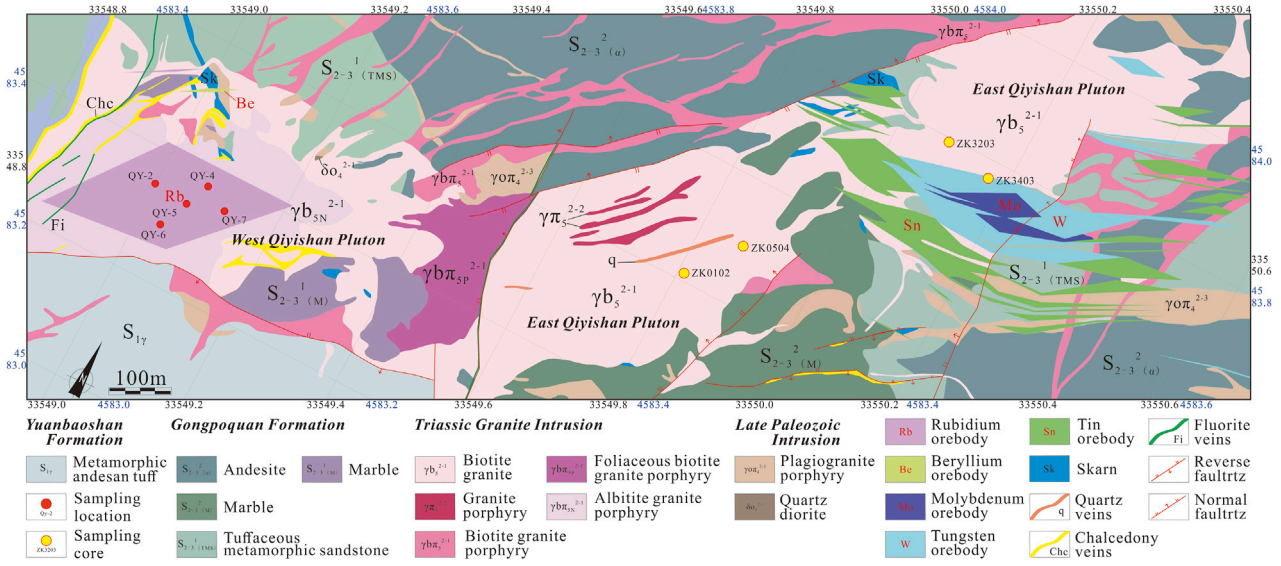

FIGURE 2
Geological maps with detailed information are available for the Qiyishan area, illustrating the precise lo-cations of the samples.

0.8 Ma (MSWD = 4.3, n = 17), and a weighted mean age of 217.4 ± 0.8 Ma (MSWD = 7, n = 17) (Figures 4C,D). These data can represent the emplacement age of the EQP.

The data points of QY-2 deviate from the concordance curves and failed to yield a concordia 206 Pb/238U age in Wetherill concordia diagram (206Pb/238U207 Pb/235U) which is mainly due to partial Pb loss and/or inherited components (Ludwig, 1998). In this case, a "Semi Total Pb/U isochron" approach can be applied for the data of sample QY-2 to obtain the diagenetic age through the lower intercept age. In a "SemiTotal-Pb/U isochron" approach, the blank-corrected data are plotted on a 2-dimensional concordia diagram (either the Tera-Wasserburg concordia), without correction for (nonblank) common Pb. If (and only if) the true Pb*/U and Pb*/Pb* isotopic ratios would yield the same, concordant ages, the data will be dispersed along a line whose Y -intercept is the 207Pb/206 pb (or 206Pb/207 Pb) of the common Pb and whose intersection with the concordia curve defines the age of the samples (Ludwig, 1998). The "Semi Total Pb/U isochron" approach has been applied by lots of researchers such as Wei et al. (2020), Song et al. (2004) and Chen et al. (2002). These studies have successfully used this method to derive credible and substantiated conclusions (Wei et al., 2020; Chun and Zhao, 2004; Song et al., 2002).

In 207Pb/206 Pb-238U/206 Pb diagram, fourteen analyzed points of sample QY-2 disperse along a line and intersect with the concordia curve, obtaining a lower intercept age of 207.5 ± 2.0 Ma (MSWD = 2.6, n = 14) (Figure 4E). As the above analysis, the lower intercept age of the sample QY-2 can represent the emplacement age of the WQP.

3.2 Major and trace element compositions

The major and trace element compositions of the bulk-rock samples from WQP (five samples) and EQP (nine samples) are shown in Supplementary Appendix B. Table. Across all samples, notable features include elevated levels of SiO2, spanning from 69.88 wt% to 79.27 wt%, and markedly minimal concentrations (<0.2 wt%) of TiO2, MnO, MgO and P2O5.

The albitite granitic porphyry WQP from the Late Triassic is mainly composed of granite and belongs to the high-K calc-alkaline series with SiO2 ranging from 69.88 wt% to 73.98 wt%, Al2O3 from 15.68 wt% to 18.59 wt%, TFeO from 0.26 wt% to 0.45 wt%, Na2O from 0.18 wt% to 6.03 wt%, K2O from 3.01 wt% to 4.78 wt% and CaO from 1.10 wt% to 1.13 wt% (Figures 5A,B). The samples also feature high levels of A/CNK, ranging from 1.11 to 1.64, exhibiting strongly peraluminous characteristics (Figure 5C). These values suggest an extremely high degree of fractionation (Figure 5D).

The biotite granite of the Late Triassic EQP primarily consists of granite and the high-K calc-alkaline series, with SiO2 ranging from 72.29 wt% to 78.91 wt%, Al2O3 from 11.31 wt% to 15.06 wt%, TFeO from 0.56 wt% to 1.63 wt%, Na2O from 3.03 wt% to 4.56 wt%, K2O from 3.41 wt% to 5.59 wt% and CaO from 0.21 wt% to 1.14 wt% (Figures 5A,B). The samples also feature high levels of A/CNK, ranging from 0.99 to 1.30, indicating metaluminous to peraluminous characteristics (Figure 5C). The points almost belong to the field of highly fractionated calc-alkaline granite (HFCG) in Figure 5D.

The major and trace element compositions of the WQP (albitite granitic porphyry) and EQP (biotite granite) samples are listed in Supplementary Appendix B. Table. There are five samples from WQP and nine samples from EQP. All samples exhibit high concentrations of SiO2, ranging from 69.88 wt% to 79.27 wt%, and extremely low concentrations (<0.2 wt%) of TiO2, MnO, MgO, and P2O5.

The albitite granitic porphyry in WQP from the Late Triassic is mainly composed of granite and belongs to the high-K calc-alkaline

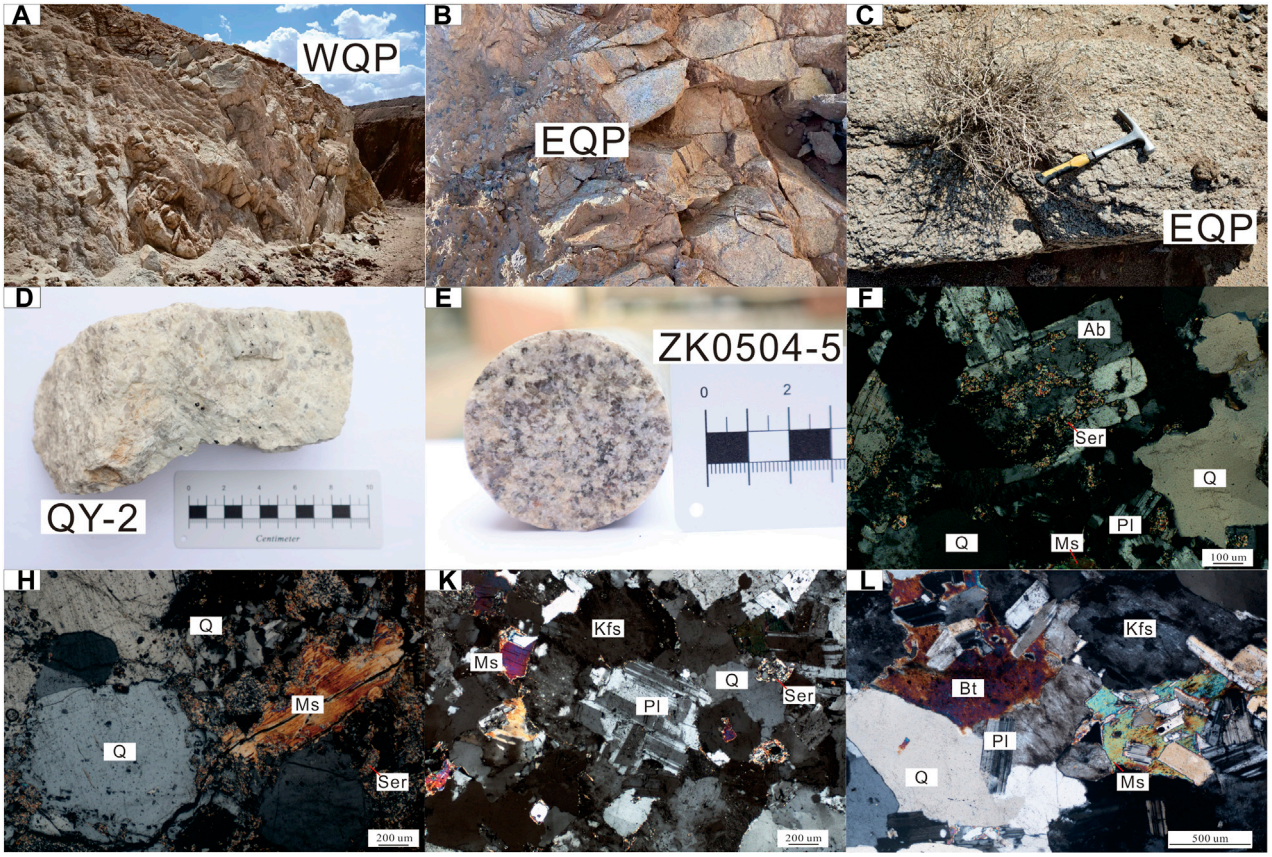

FIGURE 3
(A) The main rock outcrop of WQP in the Qiyishan area is captured in a photograph. **(B, C)** Photographs showcase the rock outcrop of EQP in the Qiyishan area. **(D)** A photograph presents a sample of albitite granitic porphyry. **(E)** Another photograph displays a sample of biotite granite. Thin section photomicrographs provide detailed views of the samples: **(F)** The photomicrograph depicts the albitite phenocryst, showing sericitization, quartz, small-grain plagioclase, and flake muscovite. **(H)** The photomicrograph focuses on the quartz phenocryst, large flake muscovite, and small-grain quartz. **(K, L)** The mineral assemblages of the biotite granite are captured in these photomicrographs. Q - quartz; Pl - plagioclase; Ab - albitite; Kfs - K-feldspar; Ser - sericite; Ms - muscovite; Bt - biotite.

series. The SiO2 content ranges from 69.88 wt% to 73.98 wt%, Al2O3 from 15.68 wt% to 18.59 wt%, TFeO from 0.26 wt% to 0.45 wt%, Na2O from 0.18 wt% to 6.03 wt%, K2O from 3.01 wt% to 4.78 wt%, and CaO from 1.10 wt% to 1.13 wt% (Figures 5A,B). The A/CNK ratio (molar Al2O3/(CaO + Na2O+ K2O)) is high, ranging from 1.11 to 1.64, indicating strongly peraluminous characteristics (Figure 5C). These values suggest an extremely high degree of fractionation (Figure 5D). The biotite granite of the Late Triassic EQP primarily consists of granite of the high-K calc-alkaline series. The SiO2 content ranges from 72.29 wt% to 78.91 wt%, Al2O3 from 11.31 wt% to 15.06 wt%, TFeO from 0.56 wt % to 1.63 wt%, Na2O from 3.03 wt% to 4.56 wt%, K2O from 3.41 wt % to 5.59 wt%, and CaO from 0.21 wt% to 1.14 wt% (Figures 5A,B). The A/CNK ratio ranges from 0.99 to 1.30, indicating metaluminous to peraluminous characteristics (Figure 5C). The data points mostly fall within the field of highly fractionated calc-alkaline granite (HFCG) in Figure 5D.

Based on the chondrite-normalized rare-earth element (REE) patterns shown in Figure 6A, the albitite granitic porphyry of WQP exhibits relatively lower ΣREE levels, ranging from 38.35 to 50.85. The REE patterns of this rock are weakly fractionated, indicated by (La/Yb)N values ranging from 1.50 to 1.92, and show strong negative Eu anomalies, with δEu values ranging from 0.03 to 0.05. On the other hand, the biotite granite of EQP demonstrates ΣREE values ranging from 37.61 to 260.17, with weakly fractionated REE patterns and (La/Yb)N values between 0.71 and 3.90. It also exhibits strong negative Eu anomalies, with δEu values ranging from 0.01 to 0.13. Although both plutons share similar rare-earth element distribution characteristics, the difference in their ΣREE and Eu anomalies may be attributed to distinct degrees of fractionation and other factors related to their geological history.

The primitive mantle-normalized spider-grams, as depicted in Figure 6B, demonstrate striking similarities between the albitite granitic porphyry of WQP and the biotite granite of EQP. Both exhibit distinct negative anomalies for Ba, Sr, P, and Ti, which indicate the occurrence of fractionation processes. Moreover, positive anomalies are observed for Th, La, Ce, and Nd. The negative Sr anomalies suggest plagioclase fractionation. These observations align with findings from previous studies investigating similar rock types and their geochemical characteristics (Miller and Mittlefehldt, 1982;

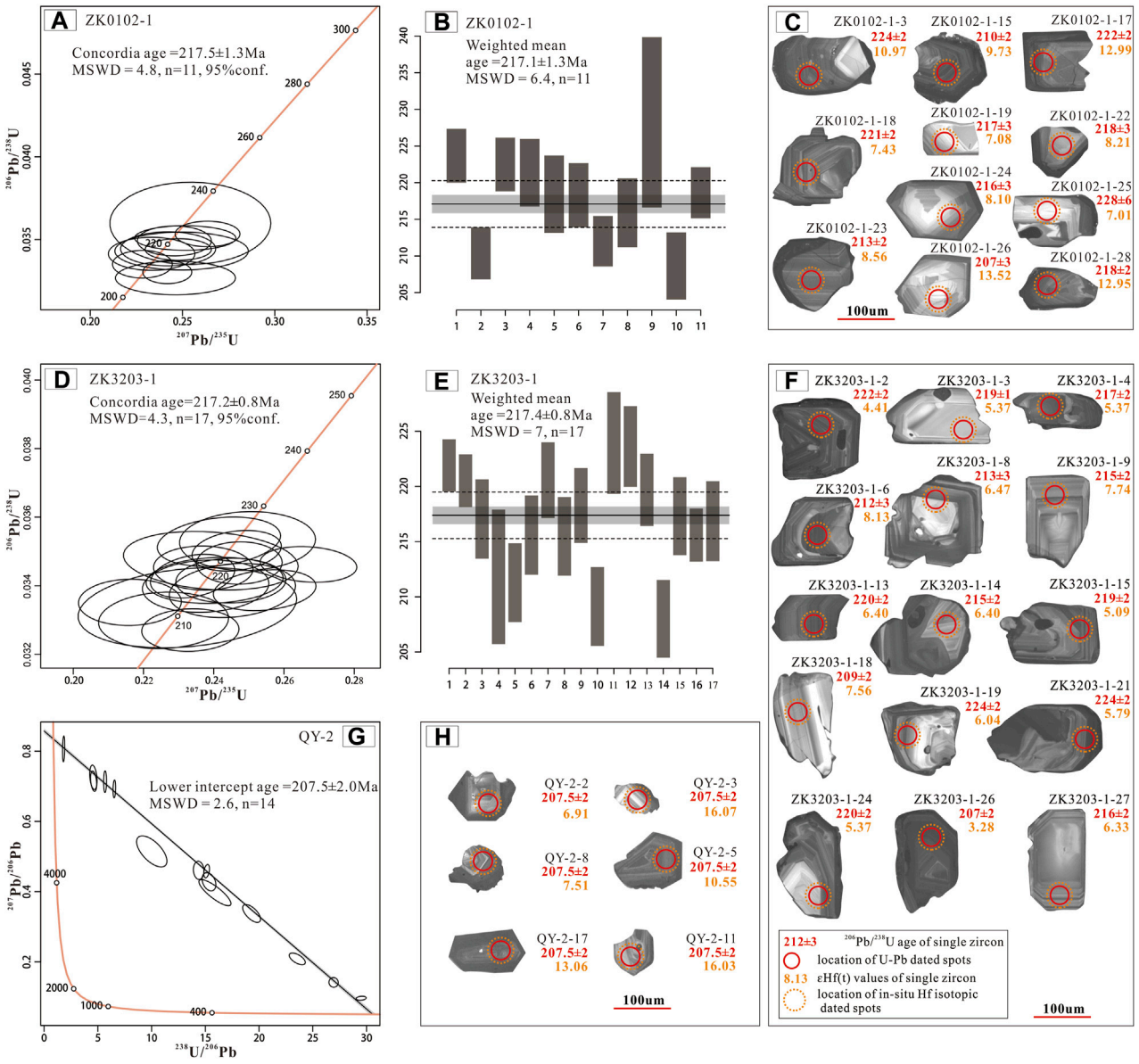

FIGURE 4
Concordia diagrams displaying zircon ages obtained through LA-ICPMS are presented as follows: **(A, B)** Concordia diagrams are shown for Sample ZK0102-1. **(D, E)** Concordia diagrams are displayed for Sample ZK3203-1 from the EQP. **(G)** The Concordia diagram represents Sample QY-2 from the WQP (Ludwig, 1998; Ludwig, 2003; Baker et al., 2004). Additionally, cathodoluminescence images **(C,F, H)** of zircon grains for ZK01021, ZK3203-1, and QY-2 are provided. The U-Pb ages (corresponding to numbers from Supplementary Appendix B. Table), the locations of the dated spots are represented by full circles on the diagrams. The site of analysis is indicated by dotted circles, within which the *in-situ* Hf isotopic compositions are depicted as εHf(t) values.

Mil et al., 1984; Li et al., 2012a; Li and Huang, 2013; Gelman et al., 2014; Wu et al., 2017a).

3.3 Whole-rock Nd isotopes

By analyzing the data presented in Table 1 and Figure 9, we can examine the Sm-Nd isotopic compositions of two samples: one from the albitite granitic porphyry of WQP and one from the biotite granite of EQP. Sample QY-2 shows an εNd(t) value of (−0.25), while sample ZK3203-1 exhibits an εNd(t) value of (−0.52). The fSm/Nd values for the granitoids are (−0.19) and 0.07, respectively. These values indicate that the granitoids have relevant two-stage Nd model ages (TDMc) ranging from 1.007 to 0.982 Ga. The slightly older crustal sources have a relatively small contribution, as suggested by the weak negative εNd(t) values (Figure 9). This information provides insights into the origin and evolution of the studied granitoids.

3.4 *In situ* zircon Hf isotopes

We conducted *in situ* zircon Hf isotopic analyses on three different samples, as shown in Supplementary Table S1 and

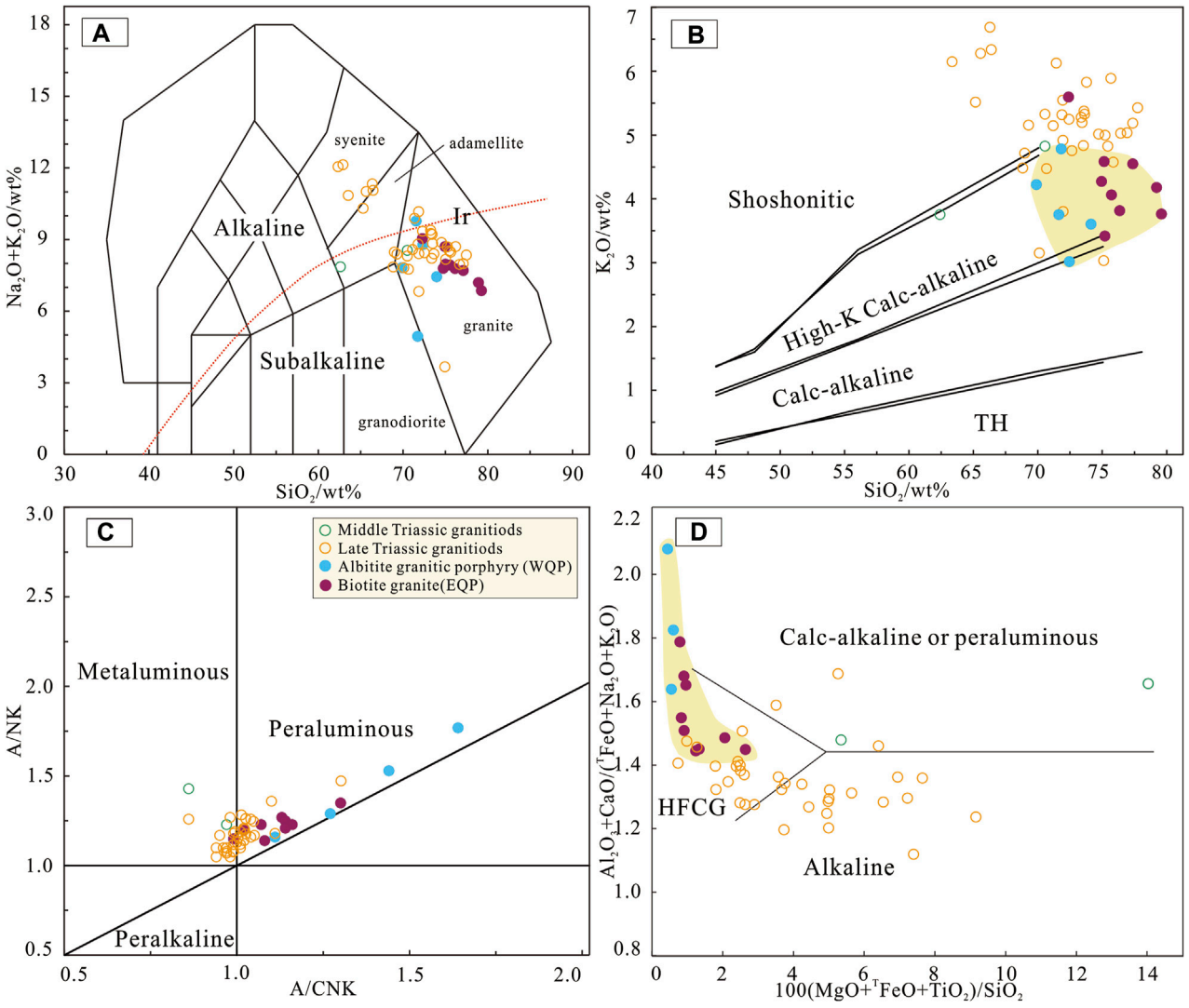

FIGURE 5
Major element diagrams for Beishan Triassic granitoids. **(A)** TAS classification diagram (after Middlemost, 1994) (Middlemost, 1994). **(B)** K2O vs. SiO2 diagram (after Peccerillo and Taylor, 1976) (Peccerillo and Taylor, 1976). **(C)** A/NK vs. A/CNK diagram (after Maniar and Piccoli, 1989) (Maniar and Piccoli, 1989). (D) ((Al2O3+CaO)/(TFeO+Na2O+K2O)) vs. (100p(MgO+TFeO+CaO)/SiO2) diagram for Triassic granitoids (after Sylvester, 1989) (Sylvester, 1989). HFCG represents highly fractionated calc-alkaline granite. TFeO is calculated as FeO +0.8998Fe2O3. A/CNK=molAl2O3/(Na2O+K2O+CaO), A/NK=molarAl2O3/(Na2O+K2O). The data used in these major element diagrams are derived from studies by Li Shan et al. (2012), Li M et al. (2020), and Peng et al. (2010), focusing on the Middle Triassic and Late Triassic granitoids in the Beishan region (Peng et al., 2010; Li et al., 2012a; Li et al., 2020).

Figure 9: one albitite granitic porphyry sample from WQP and two biotite granite samples from EQP.

Biotite granite sample ZK01021 contains 12 magmatic zircons, with a concordia 206 Pb/238U age of 217.5 ± 1.3 Ma and εHf(t) values ranging from +7.01 to +13.52. The zircons have TDMc model ages between 0.425 Ga and 0.807 Ga. Conversely, biotite granite sample ZK32031 show cases 15 magmatic zircons with a concordia 206 Pb/238U age of 217.2 ± 0.8 Ma and εHf(t) values ranging from +3.28 to +8.13. The zircons have TDMc model ages between 0.757 Ga and 1.042 Ga. Ultimately, albitite granitic porphyry sample QY-2 contains seven magmatic zircons, with a lower intercept age of 207.5 ± 2.0 Ma and εHf(t) values ranging from +6.91 to +16.07. The zircons have TDMc model ages between 0.216 Ga and 0.805 Ga.

4 Discussions

4.1 Chronology

4.1.1 Timing of granites formation and mineralization

Nie et al. (2002) acquired a Sm-Nd isochron age of 511 ± 5 Ma for fluorite and suggested that the mineralisation is related to the upward localisation and crystallographic differentiation of the Caledonian crust-mantle-derived granitic magma (Wu et al., 2007a). However, due to the lack of information on the relationship of the fluorite samples to the ore-bearing rock mass and the location of the samples, the age for fluorite might not be representative of the age of Rb-bearing rocks. The Rb-Sr isochron

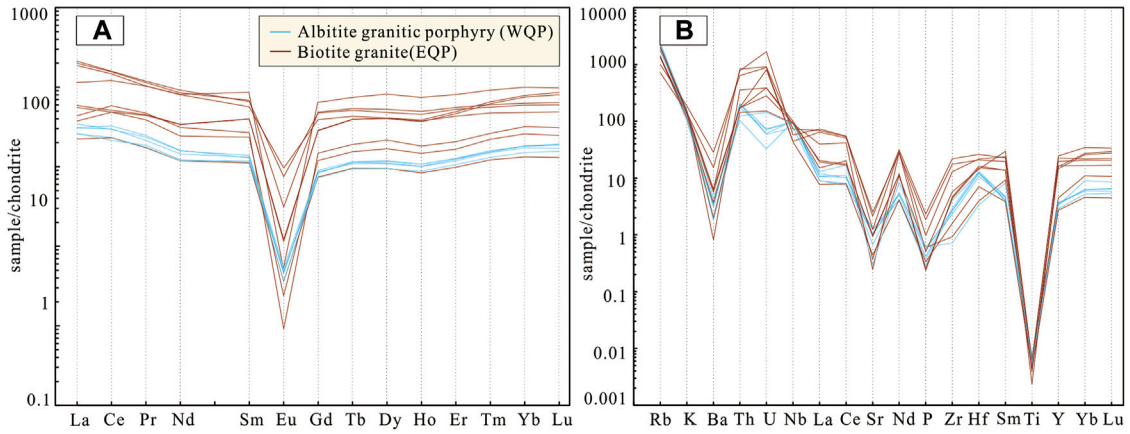

FIGURE 6
(A) The rare Earth element patterns of the WQP and EQP are chondrite-normalized. **(B)** The trace element spider diagrams of the WQP and EQP are primitive mantle-normalized. The values for chondrite and primitive mantle normalization are obtained from Sun and McDonough (1989) (Sun and McDonough, 1989).

TABLE 1 Nd isotopic data from Triassic granitoids in the Qiyishan pluton.

Nd isotopes													
No	Sample	Rock	Pluton	Age (Ma)	Sm (ppm)	Nd (ppm)	147Sm/144Nd	143Nd/144Nd	2SE	εNd (0)	fSm/Nd	εNd(t)	TDM2 (Ga)
1	QY-2	Albitite biotite granitic porphyry	West qiyishan	207.5	1.98	7.48	0.1597	0.512,575	0.000008	−1.23	−0.19	−0.25	1.007
2	ZK32031	Biotite granite	East qiyishan	217.2	13.19	37.93	0.1911	0.512,631	0.000007	−0.14	0.07	−0.52	0.982

age of 128 ± 1 Ma was determined by Lv et al. (2011) (Lv et al., 2011), implying that the alkali granite originated during the Late Yanshanian period by further differentiation of regional potassic granitic magma in a crustal extrusion-extension environment, and is closely related to rare metal mineralisation. Nevertheless, it is worth noting that the precision of the Rb-Sr isochron age might not be entirely dependable, particularly when dealing with samples that have undergone alteration (Zhao et al., 2005; Liang et al., 2020). In this case, the metallogenic age of the Qiyishan Rb polymetallic deposit remains ambiguous. As previously highlighted, a viable approach to address this issue involves conducting high-precision zircon U-Pb dating on the ore-forming rocks. Such an endeavor can yield precise and reliable data regarding the age of these rocks, as a representation of the age of mineralisation.

In this paper, LA-ICPMS zircon U-Pb dating was performed on two biotite granite samples from the EQP in Qiyishan deposit. The analysis yielded two concordia ages of 217.5 ± 1.3 Ma and 217.2 ± 0.8 Ma, representing the intrusion age of the EQP. The W-Sn-Mo quartz vein type ore bodies are located in the east of the EQP and primarily filled in the fractures of the granite bodies, indicating that the W-Sn-Mo mineralizations occurred in the post magmatic hydrothermal process and the metallogenic age is slightly posterior to the diagenetic age of the EQP.

Furthermore, a granitic porphyry sample from the WQP provided the emplacement age of 207.5 ± 2.0 Ma. For Qiyishan Rb polymetallic deposit, previous studies and the present work all show that the Rb mineralization is mainly hosted in the WQP, proven by the generally high Rb content (925.10–1,515.31 ppm) in the trace element compositions of samples from the WQP (Supplementary Appendix B. Table), and the central portion of the WQP was identified as Rb ore body (Figure 2) (Wang et al., 2009; Lv et al., 2011). The albitization is often accompanied by the occurrence of Rb mineralization (Figure 3D), which means that the Rb mineralization is the product of magmatic gas-liquid interaction that occurred in WQP. In addition, there are no veinlet Rb mineralization in the WQP or the wall rock, indicating that the Rb mineralization was not formed after magmatic intrusion. The above evidences suggest that the Rb mineralization occurs simultaneously with the magmatic intrusion process, and the zircon U-Pb age of the WQP can represent the Rb metallogenic age. In many granite-type rare metal deposits, crystallization of the pluton and the mineralization event often occur almost simultaneously (Miao, 2018; Wei et al., 2020; WuZhang et al., 2020; Wu et al., 2021b).

Based on the above analysis, we conclude that the age of Rb mineralization can be limited to 207.5± 2.0 Ma, while the age of W-Sn-Mo mineralizations is considered to be slightly younger than approximately 217 Ma.

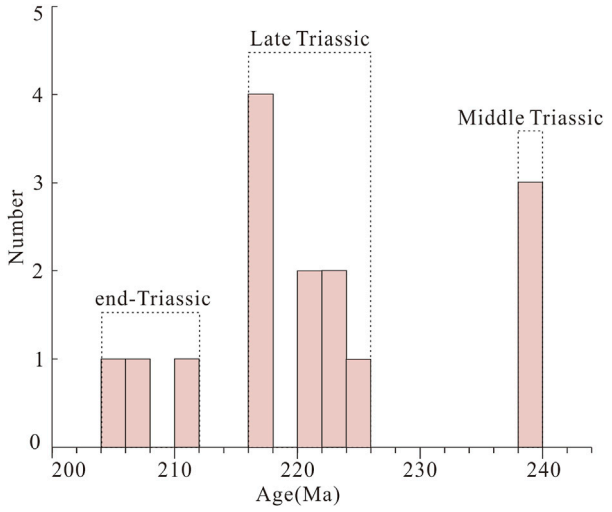

FIGURE 7
Histograms depicting the distribution of zircon U-Pb ages in the Beishan orogen presented using data sourced from Figure 1.

4.1.2 Timing of Triassic magmatism in the Beishan orogen

The Qiyishan pluton is composed of the WQP and EQP, the emplacement ages of the Qiyishan pluton are constrained to two distinct time intervals: 217.2–217.5 Ma and 207.5 Ma. These ages indicate the occurrence of two episodes of magmatic activity during the Late Triassic and End Triassic, respectively. Furthermore, the Dahuoluo pluton (240–238 Ma), located in the mid-west of the Huaniushan–Baishantang arc, represents an additional period of magmatism during the Mid Triassic. This finding, as reported by Li et al. (2012), lends support to the categorization of Triassic magmatic activity in the Beishan area into three discrete periods (Li et al., 2012c).

Upon examining the chronology of other Triassic granite formations within the Beishan region, a discernible pattern emerges. The Baixianishan, Daquan, Huaniushan, and Changliushui plutons (225–217 Ma), situated in the western part of the Huaniushan–Baishantang arc, as well as the Xiaohulishan pluton (216.9 ± 0.5 Ma) in the eastern section of the Queershan arc, were all formed during the Late Triassic (Zhang et al., 2012b; Li et al., 2012c). On the other hand, the Xiaohongshan pluton (205.9 ± 1.7 Ma, 211.8 ± 1.6 Ma), located at the center of the Xingxingxia–Hanshan block, represents magmatic activity in the End Triassic (Li et al., 2020). Consequently, we can delineate three distinct periods of magmatism in the Beishan orogen: the Mid Triassic (240–238 Ma), the Late Triassic (225–216.9 Ma), and the End Triassic (211.8–205.9 Ma) (Figure 7).

4.2 Petrogenesis

4.2.1 Types of granitoids

The granitoids identified in the Beishan area during the Triassic period manifest a transitional character, showcasing attributes reminiscent of both I-type and A-type granite (Li et al., 2012b). The main mineralogy and whole-rock chemistry of the granites from EQP and WQP are consistent with typical diamictite granites or potassium-rich granites, both of which show high SiO2 content and aluminium-rich characteristics, similar to S-type granites. Furthermore, the highly fractionated granites are also aluminium supersaturated and often contain muscovite, similar to S-type granites, they might also be highly fractionated I-types or A-types that have been affected by highly fractionation (Chappell and White, 1992a; Wu et al., 2017). In addition, the lower P2O5 content (0.01wt%~0.05wt%) and higher Na2O content of the granitoids from the WQP and EQP are significantly different from S-type granites. Therefore, the granitoids could not be classified as S-type granite (King et al., 2001).

When discriminating between A-type granite and other granite types, Whalen et al. (1987) argued that A-type granite is characterised by low Al and high Ga and Zr, thus 10,000 Ga/Al=2.6 and Zr=250ppm are proposed as the boundary between A-type and other types of granite (Whalen et al., 1987). In other words, the 10,000 Ga/Al >2.6 and Zr>250ppm are the indicators of A-type granite. The granitoids from the WQP and EQP portray 10,000 Ga/Al ratios spanning from 3.17 to 5.61, with an average of 4.62, surpassing 2.6, while the content of Zr within these granitoids varies between 8.09 ppm and 244.46 ppm, with an average of 67.92 ppm, which falls below 250 ppm (Figure 8A). The granitoids do not fully conform to the characteristics of the A-type granite.

It is important to consider that the granitoids from the WQP and EQP belong to the highly fractionated granites, and as mentioned by Wu FY. et al. (2017) (Wu et al., 2017a), in many cases, the highly fractionated granitoids also fall into the A-type granite zone due to having a high 10,000 Ga/Al ratio (Pérez et al., 2010), or A-type granites fall into the highly fractionated granite zone due to strong crystallographic differentiation (King et al., 2001).

Thus, whether the highly fractionated granites from EQP and WQP should be classified as A-type or I-type is difficult to discriminate due to the fact that A-type granite with highly fractionation share the similar mineralogical and geochemical characteristics with highly fractionated I/S-type granites (Mushkin, 2003; Wu et al., 2007a; Jia et al., 2009; Johansson et al., 2016; Wu et al., 2017a). However, Wu FY. et al. (2017) argued that A-type granite with highly fractionation is different from the characteristics of highly fractionated I/S-type granite, and gave a credible way to discriminate it (Wu et al., 2017a). Even though there is fractionation in A-type granite as well, it tends to trend on the A-type granite zones to highly differentiated granite zones. On the contrary, I/S-type granites show an opposite trend to that of A-type granites as their 10,000 Ga/Al ratios gradually increase during the process of differentiation (Figure 8A). The highly fractionated granites from EQP and WQP exhibit characteristics particularly similar to those of I/S fractionated granites.

In addition, Wu FY. et al. (2017) collected and collated data from a large number of A-type granites and I/S fractionated granites (Figure 8B) (Wu et al., 2017a). It could be observed that there is an overlap between the positions occupied by these two granites in the diagram, and the granites in the overlapping positions show transitional features between A-type granites and I/S fractionated

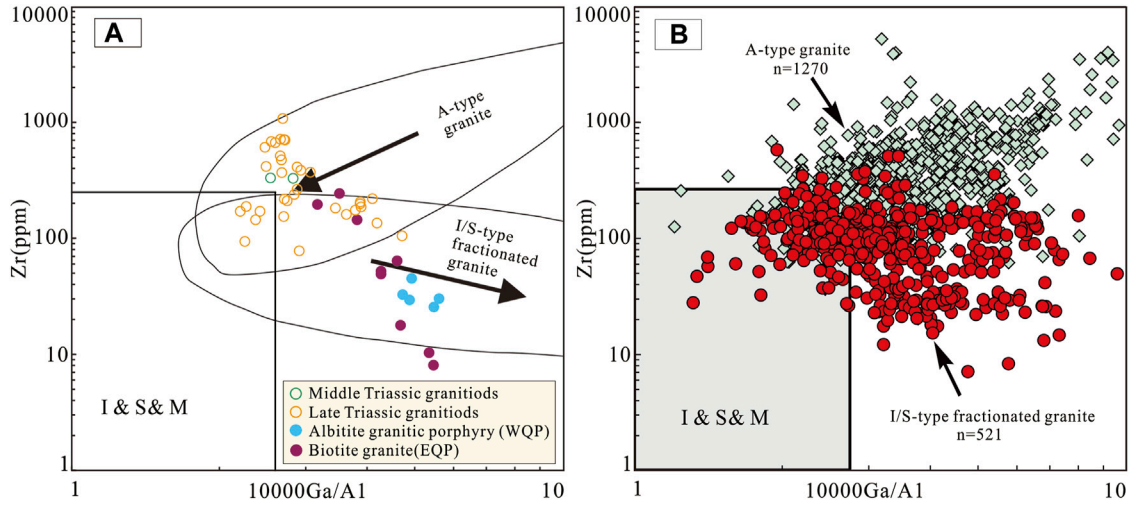

FIGURE 8
(A) Zr content vs. 10,000*Ga/Al diagrams, illustration of the differentiation between A-type granite and highly differentiated granite (modified by Wu et al. (2017)); **(B)** Zr content vs. 10,000*Ga/Al diagrams with data of a large number of A-type granites and I/S fractionated granites from Wu et al. (2017) (Wu et al., 2017a).

granites. In fact, the highly fractionated granites from EQP and WQP fall partly in this overlap area in Figure 8, suggesting that some degree of transitional features are also present in the granites. This is not an isolated case in the surrounding area of the Qiyishan deposit, the granites of regional contemporaneity in Beishan orogen have also been studied by previous generations, Li S. et al. (2012) suggested that Daquan (221 Ma), Huaniushan (221-217 Ma), Changliushui (223 Ma) and Baixianishan (224 Ma) granites are mainly highly fractionated I-type granite with some transitional features to A-type (Figure 12) (Li et al., 2012a).

Based on above analysis, we tend to consider that the granites generally show the characteristics of the highly fractionated I-type granite, and are also characterised by a transition to A-type like granites to some extent.

4.2.2 Source regions

The compositional characteristics of rocks inherit the properties of their source regions, which can be inferred from the geochemical features of major and trace elements in the rocks (Li et al., 2012c). The Triassic granitoids discovered in the WQP and EQP regions exhibit elevated concentrations of Y ranging from 15.17 ppm to 111.98 ppm, with an average of 45.97 ppm. They also display low Mg# values ranging from 0.11 to 72, with an average of 0.37, and low Sr/Y ratios ranging from 0.05 to 1.70, with an average of 0.76. These characteristics align with the granitic properties of a young basaltic lower crust, which is typically enriched in Y and exhibits low Mg# values and Sr/Y ratios (Chen and Arakawa, 2005).

Accurate identification of source regions relies on the analysis of Nd isotopic and zircon Hf isotopic signatures (Li et al., 2002; Wu et al., 2007a; Bouvier et al., 2008). In the case of the Triassic granitoids from sample ZK0102-1 in the EQP, zircon εHf(t) values exhibit a positive range of +7.01 to +13.52, and the Hf model ages (TDMc) indicate relatively young values ranging from 0.425 Ga to 0.807 Ga. Besides, the granitoids from sample ZK3203-1, also from the same pluton, display positive zircon εHf(t) values ranging from +3.08 to +8.13 and even younger Hf model ages (TDMc) ranging from 0.757 Ga to 1.042 Ga. This discrepancy in Hf isotope characteristics can be attributed to their distinct sampling locations (Figure 2). However, despite this difference, the zircon Hf isotopic signatures of both samples suggest that the source region consists of juvenile mantle materials. Moreover, the sample ZK0102-1 indicate the utilization of significantly younger mantle-derived materials (Bleousova et al., 2006).

The Triassic granitoids from sample QY-2, situated in the WQP, display positive zircon εHf(t) values ranging from +6.91 to +16.07. Furthermore, their Hf model ages (TDMc) range from 0.216 Ga to 0.805 Ga, which aligns closely with the formation age of the granitoids. These observations suggest that the source region of these granitoids underwent recent development and that the zircon Hf isotopic signatures indicate the utilization of juvenile mantle-derived materials (Bleousova et al., 2006; Wu et al., 2007a).

The Triassic granitoids found in the WQP and EQP exhibit weakly negative εNd(t) values of (−0.25 and −0.52, respectively) and Nd model ages (TDMc) ranging from 0.998 Ga to 1.007 Ga, indicating the involvement of slightly older crustal sources. The presence of crustal contamination during the emplacement of magma can result in biased, negative Nd isotope values. These findings suggest that the granitoids possess mixed sources, including mantle-derived materials and slightly ancient crustal components (Figure 9).

Although high positive εHf(t) values and slightly negative εNd(t) values appear in the same rock masses, the differences in Nd-Hf isotopic composition between zircon and whole rock need to be considered. The zircon Hf isotope data represents the source region characteristic of the early zircon crystallisation, while the Nd isotope data of bulk rocks are more likely influenced by mixing/assimilation during magma evolution, and therefore cause the different Hf-Nd isotope data. However, considering the Hf-Nd isotopic signature as well as major and trace geochemical studies, this does not affect the

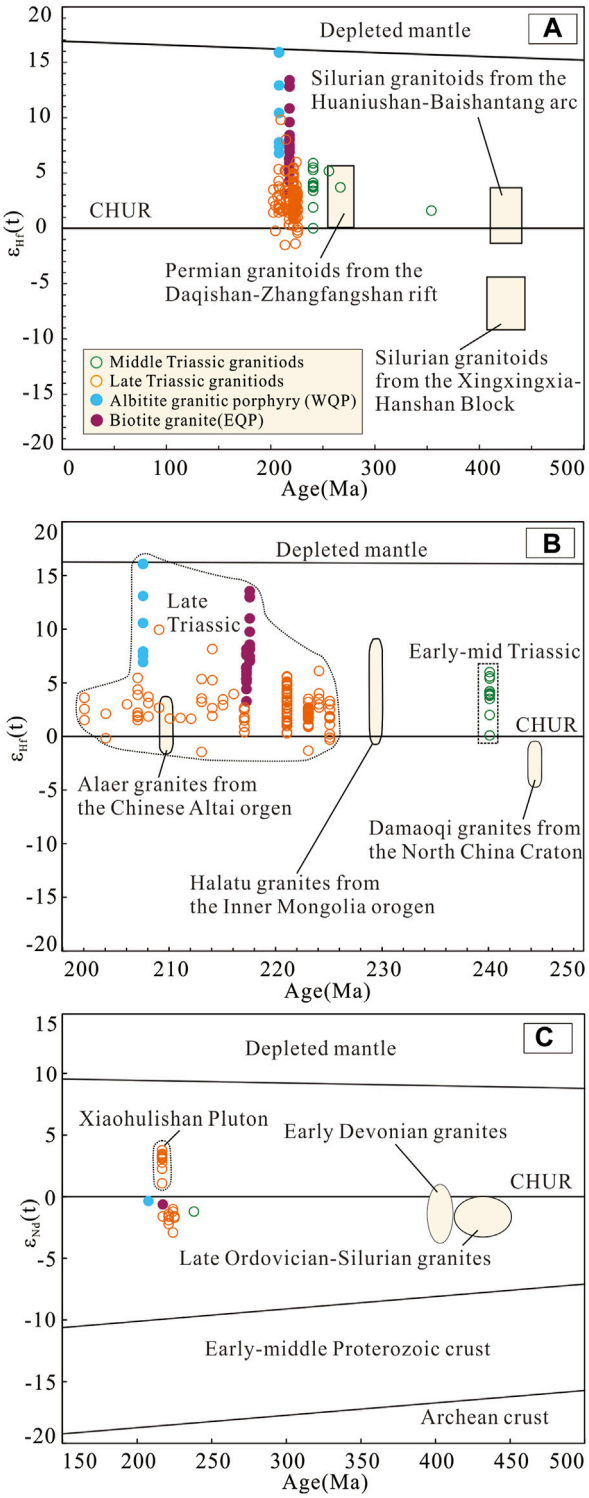

FIGURE 9
(A) The εHf(t) vs. age diagram includes the following data sources: Data for the Permian granitoids from the Daqishan-Zhangfangshan rift, Silurian granitoids from the Huaniushan-Baishantang arc, and the Xingxingxia-Hanshan block are obtained from Mao et al. (2009), Liu Y. et al. (2010), and Zhang et al. (2010b), respectively (Mao et al., 2009; Liu et al., 2010; Zhang et al., 2010). **(B)** The εHf(t) vs. age diagram includes the following data sources: Data for the Alaer granites from the Chinese Altai orogen, Halatu granites from Inner Mongolia, and Damaoqi granites from the North China Craton are derived from Chen et al. (2009), Wang et al. (2008b), and Zhang et al. (2010a), respectively (*Continued*)

FIGURE 9 (Continued)
(Wang et al., 2008b; Chen et al., 2009; Zhang et al., 2010a). **(C)** The εNd(t) vs. age diagram includes the following data: Data for the Early Devonian granite from Li et al. (2009, 2011) (Li et al., 2009b; Li et al., 2011)and Late Ordovician to Silurian granites from Zhao et al. (2007) and Mao et al. (2009) (Zhao et al., 2007; Mao et al., 2009). Additionally, data for the Dahuoluo Pluton, Daquan Pluton, Huaniushan Pluton, Changliushui Pluton, and Baixianishan Pluton are sourced from Li Shan et al. (2012) (Li et al., 2012a), data for the Xiaohulishan Pluton are from Wei (2019) (Ouxiang, 2019), and data for the Xiaohongshan Pluton are from Li M et al. (2020) (Li et al., 2020).

conclusion that the Qiyishan granitoids originated from a mixed crust-mantle source.

The absence of mafic rocks or dark ferrimafic inclusions in the study area, combined with the high SiO2 concentrations and low MgO and Cr concentrations of all samples from the WQP and EQP, supports the conclusion of a mixed source for the Triassic granitoids. This mixed source is likely the result of the emplacement of mantle-derived mafic magmas into the lower crust (Whalen et al., 1987; Wu et al., 2002).

In the Beishan orogen, granites with the characteristics of a crust-mantle mixing source area are widely distributed. For example, Li S. et al. (2012) suggested that the Hf-Nd isotopes features of Daquan (221 Ma), Huaniushan (221-217 Ma), Changliushui (223 Ma) and Baixianishan (224 Ma) granites indicate a mixed source for the granitoids (Li et al., 2012a). Besides, the Xiaohulishan, Baishan, Huaheitan, Donggebi and Xioabaishitou plutons are considered to originate from a mixed crust-mantle source (Peng et al., 2010; Yang et al., 2012; Wu et al., 2017b). The above contemporaneous plutons share similar source characteristics with the granitoids investigated in this study, which laterally supports that the Qiyishan pluton may also originate from crust-mantle mixing sources.

4.2.3 Fractional crystallisation

The granitoids from the WQP and EQP in the Beishan orogen are spatially separated by the NS fault. The emplacement age of the WQP is constrained to the Late Triassic period (207.5 Ma), while the EQP's emplacement age falls within the End Triassic period (217.5–217.2 Ma). Despite their temporal separation, the major and trace element compositions of the granitoids found in both plutons exhibit relatively similar characteristics.

The granitoids display a high degree of fractionation, as evidenced by several factors. There is a decrease in the total rare Earth element (∑REE) concentrations and the normalized ratio of (La/Yb)N, along with an increase in negative Eu anomalies. Additionally, the presence of tetrad effects is observed (Figures 5, 6) (Miller and Mittlefehldt, 1982; Mil et al., 1984; Li and Huang, 2013; Gelman et al., 2014). The geochemical features suggest a significant degree of differentiation and fractionation within the granites during their magmatic evolution.

The negative Eu anomaly observed in the Triassic granitoids from the WQP and EQP indicates the preferential separation of plagioclase feldspar during the crystallization process. This phenomenon is attributed to the fractionation of Eu, which is incorporated into the crystal lattice of plagioclase. Additionally, the decrease in concentrations of Ba and Sr, along with the

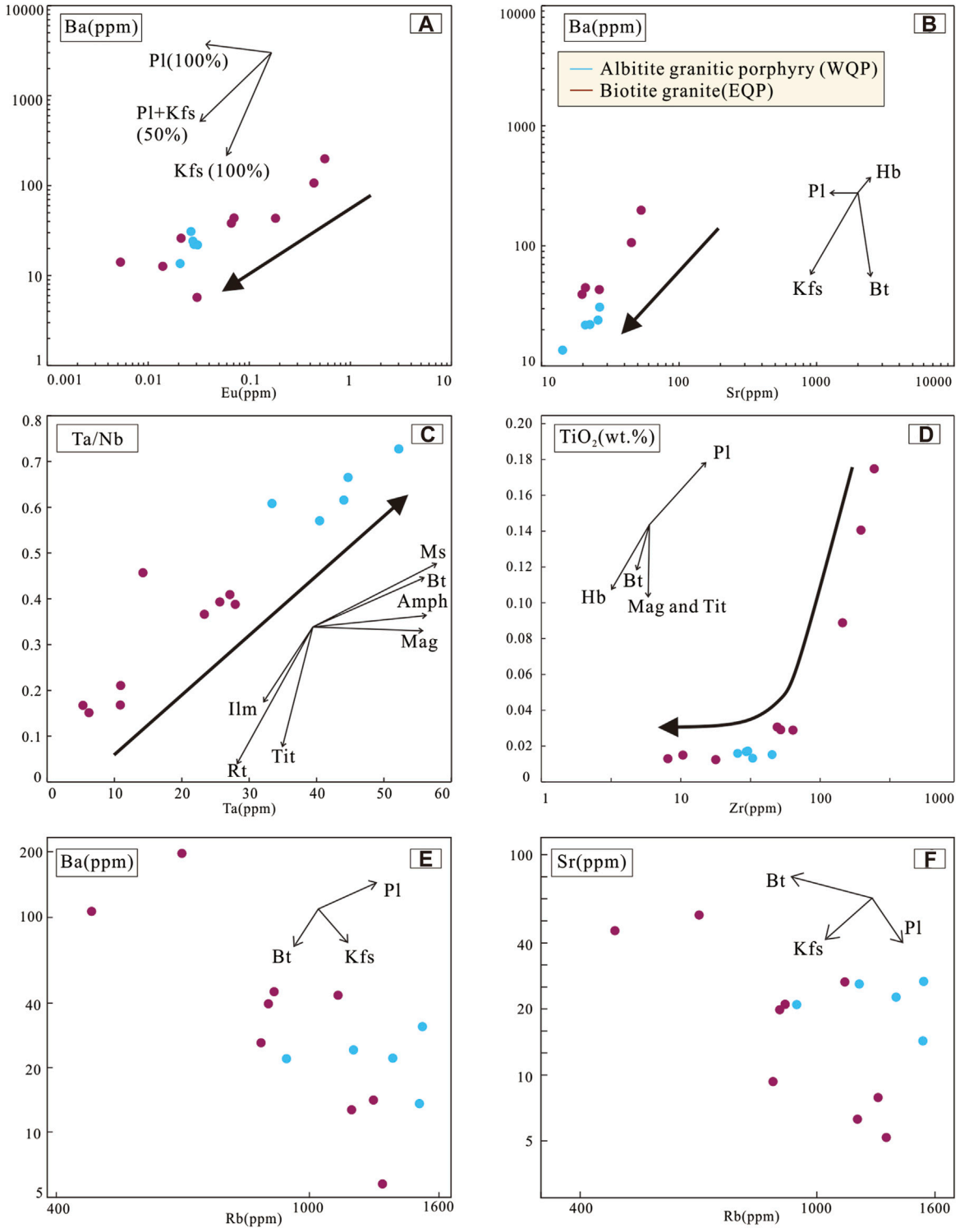

FIGURE.10
(A) Ba vs. Eu, **(B)** Ba vs. Sr, **(C)** Ta/Nb vs. Ta, **(D)** TiO2(wt%) vs. Zr, **(E)** Rb vs. Ba, **(F)** Rb vs. Sr diagrams showing fractionation of plagioclase (Pl), K-feldspar (Kfs), clinopyroxene (Cpx), biotite (Bt), muscovite (Ms), amphibole (Amph), ilmenite (Ilm), rutile (Rt), titanite (Tit), magnetite (Mag), hornblende (Hb) (modified by Qiu L et al. (2014) (Qiu et al., 2014).

increasing negative Eu anomaly, suggests a common process of segregation and crystallization of both K-feldspar and plagioclase feldspar in these granitoids (Figures 10A,B). In addition, it is recognized that the Rb–Ba and Rb–Sr variations (Figures 10E,F) and strongly negative Ba, Nb, Sr, P and Ti anomalies (Figure 6B) shows the fractionation of biotite, K-feldspar and plagioclase for granites (Qiu et al., 2014). This evidence further supports the occurrence of fractional crystallization and differentiation during

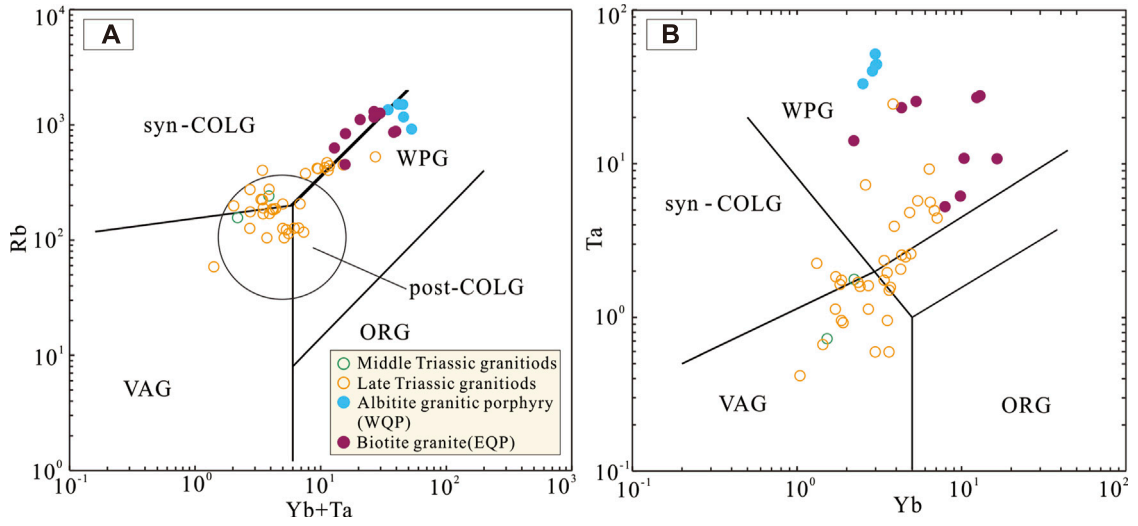

FIGURE 11
Tectonic discrimination diagrams for Triassic granitoids in the Beishan orogen. **(A)** (Y+Nb)-Rb, **(B)** Yb-Ta diagram (modfied by Pearce et al., 1984) (Julian et al., 1984), VAG: Volcanic arc granites; WPG: within plate granites; Syn-COLG: Syn-collision granites; post-COLG: post collision granites; ORG: ocean ridge granites.

the magmatic evolution of the Triassic granitoids in the WQP and EQP. The negative anomaly of P may have arisen from the segregated crystallisation of apatite, while the negative anomaly of Ti could be associated with the segregated crystallisation of the Ti-rich mineral phase. Fractionation of biotite, according to Stepanov et al. (2014) (Stepanov et al., 2014), can increase the Ta concentration and Ta/Nb ratio and decrease the TiO2 concentration of the granite. Therefore, the observed variations in the Ta/Nb ratios coupled with Ta concentrations in the granites may have resulted from biotite fractionation (Figure 10C). Additionally, the decrease in Zr, which correlates with a decline in the TiO2 concentration, suggests the segregated crystallisation of amphibole and/or biotite (Figure 10D).

While the granitoids from the WQP and EQP share similar geochemical characteristics, it is crucial to emphasize that they do not originate from the same magmatic period. These granitoids represent distinct stages of evolution during different time periods, specifically from the Late Triassic to the End Triassic.

Magma evolution over a timespan as extensive as 10 Ma is relatively uncommon. Current experimental simulations and theoretical calculations indicate that the duration from magma formation to the closure of zircon U–Pb isotope system within a single intrusion typically does not exceed 1 Ma (Pitcher, 1997; PetfordN et al., 2000; Petford, 2003). Therefore, the presence of a10 Ma interval between the WQP and EQP strongly implies that they were not derived from the same magma crystallization event. Rather, it is plausible that they originated from distinct batches of magma emplacement from similar source regions (Coleman et al., 2004; Wu et al., 2007a). This interpretation provides further validation for the observed compositional differences between the two magma source regions.

The Zr/Hf and Y/Ho ratios are indicative of the degree of fractional crystallisation of magma, and significant changes in these ratios signify alterations in magma characteristics due to differentiation (Pérez et al., 2010; Ballouard et al., 2016). In the case of the WQP and EQP samples, their Zr/Hf ratios span from 11.66 to 7.77 and 30.52 to 7.73, respectively. Meanwhile, the Y/Ho ratios observed in the WQP and EQP samples exhibit ranges of 29.49 to 26.09 and 36.56 to 18.09, respectively. The shifts in the Zr/Hf and Y/Ho ratios within the granitoids from the WQP and EQP do not follow a continuous pattern, signifying that their evolution is not continuous. Consequently, the EQP and WQP cannot be attributed to the products of an ongoing magmatic evolution within the same magmatic period. The presence of highly differentiated granites within the EQP implies that the magmatic activity persisted to an advanced stage in the Late Triassic magmatic period (217.5–217.2 Ma).

In summary, the WQP and EQP are products of magmatic activity occurring in distinct periods, stemming from similar source regions and undergoing similar fractional crystallisation processes.

4.2.4 Magmatic fluid interaction

Although the granites have underwent the highly fractional crystallisation, but it is noticed that the granite samples are too rich from the K2O and SiO2, and there is a minor negative trend between these two data (Figure 5B), suggesting that the granites from the EQP and WQP were not only affected by fractional crystallisation, but also underwent magma-hydrothermal transition stages and have been modified by later fluid action (Wu FY. et al., 2017) (Wu et al., 2017a).

Bau (1996) and Ballouard et al. (2016) suggested that Zr/Hf=26, Nb/Ta=5 can be used to classify peraluminous granites into normal crystallographic differentiation and magmatic-hydrothermal interaction (Bau, 1996; Ballouard et al., 2016). The granites from EQP have Nb/Ta values (average 3.97) less than 5 and Zr/Hf values (average 15.80) less than 26, while the granites from WQP have Nb/Ta values (average 1.58) much less than 5 and Zr/Hf values (average 8.68) much less than 26, reflecting that both WQP and EQP underwent magma-

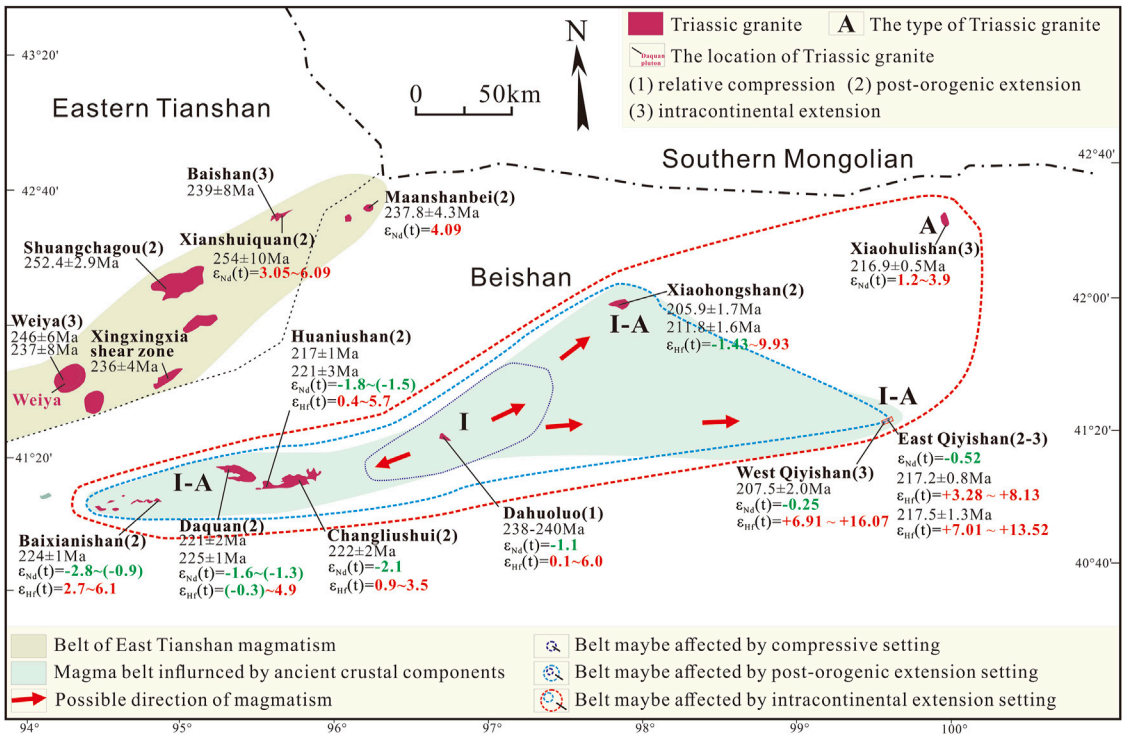

FIGURE 12
A schematic cartoon is presented, illustrating the spatial distribution, ages, εHf(t), εNd(t) values, and tectonic setting stages of the Triassic plutons in the Beishan orogen and adjacent areas. The schematic is modified based on the works of Li et al. (2009), Wang et al. (2007), and Li Shan et al. (2012) (Wang et al., 2007; Li et al., 2009b; Li et al., 2012a). The data utilized in the schematic are sourced from various references, including Li et al. (2006), Li Shan et al. (2012), Li M et al. (2020), Liu et al. (2005), Tang et al. (2007), Wang et al. (2010), Zhang Z. Z. et al. (2005), Zhang et al. (2012b), Zhou TF et al. (2010), and this article (Nie et al., 2002a; Zhang et al., 2005b; Liu et al., 2005; Tang et al., 2007; Wang et al., 2010; Zhou et al., 2010; Li et al., 2012a; Zhang et al., 2012b; Li et al., 2020).

hydrothermal transition stages and melt-fluid interactions occurred in both granites. Comparatively, the melt-fluid interactions in the WQP are more intense than that of the EQP (Yuan and Zhao, 2021; Zhao et al., 2022).

In addition, Granite magma will lead to a significant decrease in trace elements such as Cr, Ni, Co, Sr, Ba and Zr during fractional crystallisation (Gelman et al., 2014). However, in the late stages of magmatic differentiation, fluid action can lead to a more pronounced lack of Ba, Sr (Jahn et al., 2001). Wu et al. (2020, 2023) reported the Ba content (average 289 ppm), Sr content (average 137 ppm) of Highly fractionated Himalayan granites, and Sr content (average 84 ppm) of Highly fractionated Nanling granites (Wu et al., 2020; Wu et al., 2023). In comparison, the Ba content (5.71–198.45 ppm, average 54.58 ppm) and Sr content (5.18–53.07 ppm, average 21.51 ppm) of EQP samples, the Ba content (13.55–30.90 ppm, average 22.52 ppm) and Sr content (14.21–26.44 ppm, average 21.94 ppm) of WQP samples are significantly lower, suggesting that there are stronger Ba, Sr deficits in EQP and WQP. It is inferred that the granites may have been modified by later fluid action.

4.3 Tectonic setting

Following the closure of the Palaeo-Asian Ocean in the Mesozoic-Cenozoic era, the Beishan Orogenic Belt and the Central Asian Orogenic Belt underwent intense compression and thrusting, entering a phase of intracontinental evolution (Zuo and He, 1990a; Zuo et al., 1990b; Liu and Wang, 1995; Dumitru and Hendrix, 2001; Gong et al., 2002; Gong et al., 2003; Zuo et al., 2003; Zhang et al., 2005a; Xiao et al., 2010a; Xiao et al., 2010b; He et al., 2014; Shi et al., 2019). The uplift of the Shalazha Mountain, situated in the eastern part of the Beishan orogen, is associated with the intracontinental orogenesis of the CAOB during the Late Triassic period (Peng et al., 2023). In the Beishan region, three distinct phases of folding and rapid exhumation occurred around 225–180 Ma, 130–95 Ma, and 75–60 Ma (Tian et al., 2016; Gillespie et al., 2017).

In the Qiyishan deposit, the granitoids in the WQP and EQP are classified as highly fractionated I-type granite with a transition to A-type like granite. In most cases, A-type granite are emplaced extensional tectonic environments, signifying the conclusion of an orogenic cycle (CollinsW et al., 1982; Clemens et al., 1986; Whalen et al., 1987; Eby, 1990; Eby, 1992; Hong et al., 1995; Yang et al., 2006; Wu et al., 2007b; Ding et al., 2011; Chen et al., 2013). This suggests that granites from the WQP and EQP might have formed at a stage when the tectonic environment was in transition.

The Triassic granitoids from the WQP and EQP are primarily categorized as within-plate granites (WPG) based on their positions in the (Y + Nb) Rb and Yb-Ta diagrams (Figures 11A,B). However, certain Triassic granites from the EQP exhibit positions in the transitional field between post-collision granites and WPG

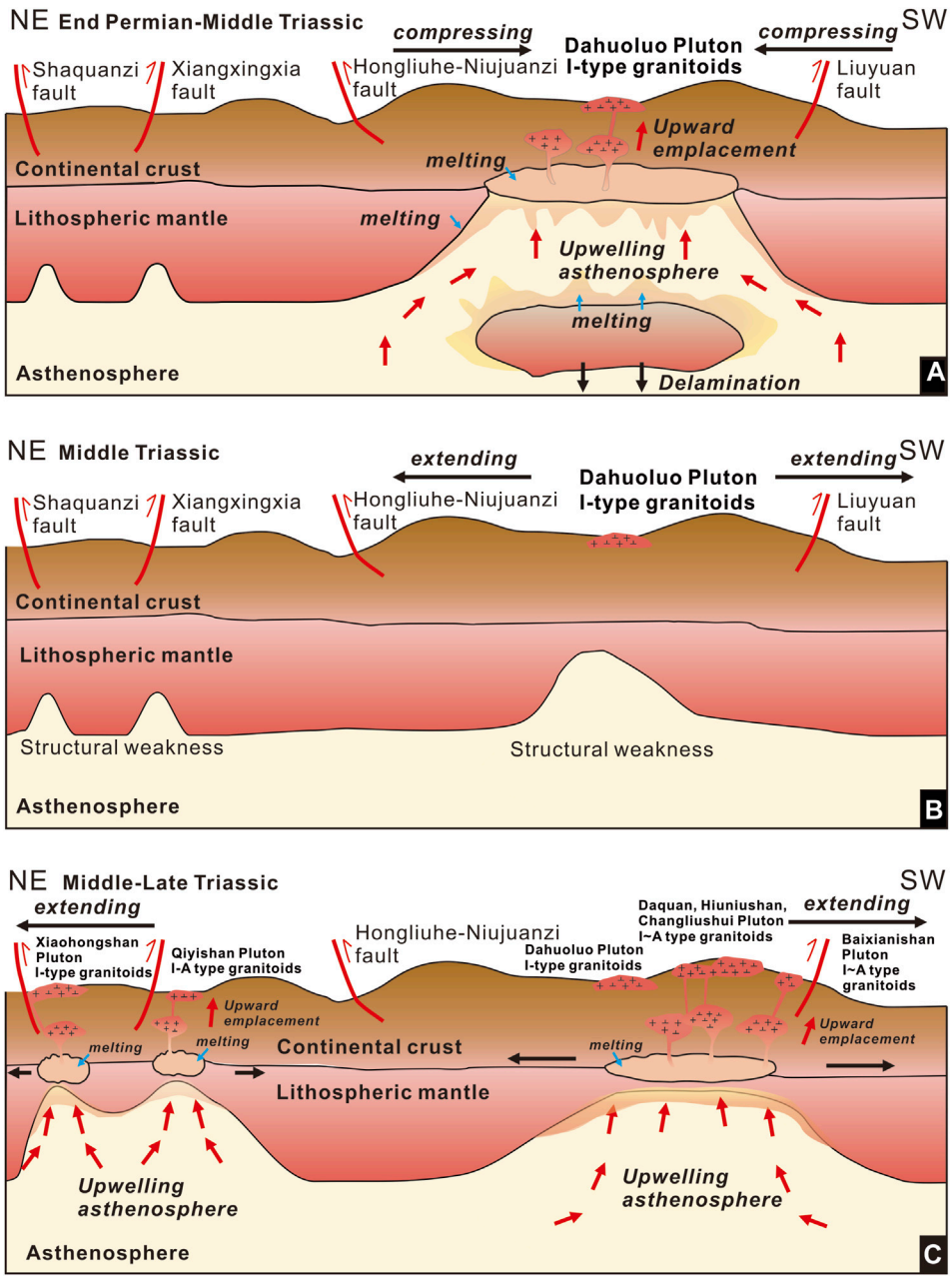

FIGURE 13
A modified schematic cartoon is provided to illustrate the tectonic evolution and petrogenetic model of the south-central margin of the Beishan orogen from the **(A)** End Permian-Middle Triassic, **(B)** Middle Triassic to **(C)** Middle -Late Triassic. The schematic is based on the work of Li Shan et al. (2012) (Li et al., 2012a). It is worth mentioning that the illustrations are not drawn to scale.

(Figure 11A). This suggests that these particular granites were emplaced in a transitional tectonic environment during the transition from post-orogenic to intracontinental extensional tectonics.

As established in prior studies, the WQP is the ore-bearing pluton of the Qiyishan Rb polymetallic deposit. Around 207 Ma, a notable shift occurred in the regional tectonic context, transitioning from post-orogenic to intracontinental extensional tectonics. Concurrently influenced by mantle subduction, the Rb-bearing parent magma was intruded upwards from the magma source area along the regional deep major fracture. Throughout this ascent, the parent magma underwent substantial differentiation, resulting in the enrichment of Rb for subsequent mineralization processes. Ultimately, this intricate geological process gave rise to the formation of the Qiyishan Rb-bearing pluton.

During the Paleozoic orogeny, the evolution of the Beishan orogenic collage prior to the Triassic was marked by the formation of multiple Early to Mid-Paleozoic arcs across different regions of the Palaeo-Asian Ocean (Peng et al., 2010). The closure of the Palaeo-Asian Ocean signified the culmination of orogenic processes and the ultimate configuration of the orogen. Supported by the

subsequent evidence, it can be deduced that the closure of the Palaeo-Asian Ocean occurred no later than the Triassic period.

The closure of the Hongliuhe-Niujuanzi-Xichangjing ocean is widely attributed to the Late Permian to Early Triassic. This conclusion is drawn from several lines of evidence, including the existence of the Baihu Basin, a foreland basin formed due to the collision between the Gongpoquan arc and Shuangyingshan arc. The assessment is further variations in provenance, and changes in paleogeography substantiated by the analysis of sedimentary sequences (Wang et al., 2021).

Furthermore, Song D. F. et al. (2018) conducted 40Ar/39Ar chronology analysis in the central Beishan area, yielding crucial insights into the ages of metamorphic-deformation complexes. These ages range from 323.1 ± 3.6 Ma to 209.2 ± 4.0 Ma, progressing from the northern to southern regions (Song et al., 2018). This data signifies the persistence of ductile deformation in the central Beishan area, spanning from the early Carboniferous to the Late Triassic. The consistent pattern of deformation, coupled with the decreasing ages in the southward direction, implies an ongoing accretion of the orogenic belt from north to south. This implies a likely extension of orogenic processes into the Triassic period in the central Beishan area.

Lastly, the presence of Early-Mid Triassic clastic rocks unconformably overlying Late Permian sandstone in the Niujuanzi ophiolitic mélange indicates the occurrence of Early Triassic tectonic events (Tian et al., 2014). Furthermore, Permian-Triassic arc-related sediments found in the Hongyanjing Basin, located near the Xingxingxia Fault zone, exhibit folding and deformation occurring in two stages throughout the Late Permian to Late Triassic period, approximately 250,219 Ma (Tian et al., 2015). Collectively, the geological records strongly support the conclusion that the closure of the Palaeo-Asian Ocean occurred no later than the Triassic period.

The analysis provided above underscores the significant role of the Triassic period in the evolution of the Beishan orogenic belt. This era emerges as a pivotal phase characterized by the ultimate amalgamation of the southern active margin of the Siberia Craton and the passive margin of the Tarim Craton (Xiao et al., 2009; Li et al., 2012a). Additionally, the Triassic period marked the transition of the orogenic belt into a phase of intracontinental extension. The granites identified within the EQP play a crucial role in indicating this transition from a post-orogenic to an intracontinental extensional setting. These granites offer compelling evidence to support the shift in the tectonic environment during the Triassic period.

4.4 Triassic magmatism and tectonism evolution

In continental regions, the occurrence of an intracontinental extensional tectonic setting is often associated with intracontinental orogeny. This process typically originates from the delamination of the lithospheric mantle, followed by the upwelling of the asthenosphere. The interaction between high-temperature mantle heat flow and the lower crust of the initial orogenic belt triggers the tensile reactivation of the original extrusion orogenic belt. Consequently, partial melting and extension occur, resulting in extensional intracontinental orogeny within the structural weaknesses of the paleosuture zone (Zheng and Chen, 2017; Zheng and Chen, 2021; Zheng et al., 2022; Zheng, 2023). Additionally, continental active splitting can be induced by processes such as plate rewind and plate breakage (Zheng, 2023).

The summary of the magmatic and tectonic evolution of the Triassic pluton in the Beishan orogen, illustrated in Figures 12, 13, is as follows. During the period of final amalgamation from the end of the Permian to the middle of the Triassic, the crust of the Beishan orogen likely experienced thickening. This thickened lower crust may have become gravitationally unstable, resulting in lithospheric delamination and upwelling of the asthenosphere (Xiao et al., 2009; Li et al., 2012a).

The heating at the base of the lower crust would have been induced by above process, resulting in partial melting (Figure 13A). Consequently, the Dahuoluo pluton would have experienced the generation of adakitic magma and/or I-type granitic magma (Xiao et al., 2009; Li et al., 2012a). The Mid Triassic magmatism associated with the Dahuoluo pluton occurred in a compressive environment and was situated at the central region of the Beishan Triassic magmatic belt (Figure 12). Following the completion of the amalgamation, the tectonic regime transitioned to an extensional setting (Figure 13B).

During the middle to late Triassic, within the southwestern expanse of the Dahuoluo pluton, the subsiding delaminated lithosphere coupled with the upsurge of asthenosphere led to partial melting of the crust. This process gave rise to the formation of highly fractionated I-type granites, which progressively exhibited traits transitioning towards A-type granites.

The Daquan, Huaniushan, Changliushui, and Baixianishan plutons, which consist of granites, are thought to have originated within a post-orogenic extensional environment (Figure 13C) (Li. et al., 2012a).

In the northeastern region of the Dahuoluo pluton, namely, the Xiaohongshan, East Qiyishan, West Qiyishan, and Xiaohulihsan plutons, the tectonic environment transitioned from a post-orogenic to an intracontinental extensional setting (Peng et al., 2010; Zhang et al., 2012b; Li et al., 2020). The formation of these plutons can be attributed to asthenospheric upwelling, which induced partial melting of the crust within the structural weaknesses of the paleosuture zone (Zheng and Chen, 2017; Zheng and Chen, 2021; Zheng et al., 2022; Zheng, 2023). Along the northeast direction, the granites within these plutons exhibit a transition from I-type to A-type, accompanied by changes in εNd(t) values from negative to positive. These transformations indicate a decrease in the contribution of ancient crustal components to the magma source (Figure 12; Figure 13C).

In summary, the WQP and EQP represent magmatic products from different periods but originating from similar source regions. These source regions were formed due to asthenospheric upwelling in the structural weaknesses of the paleosuture zone, resulting in partial melting of the crust. Subsequently, both plutons underwent fractional crystallization and crustal contamination during their emplacement.

The εNd(t) values of the Xiaohulishan plutons are positive and relatively uniform, demonstrating similarity to the Maanshanbei and Xianshuiquan plutons in the East Tianshan area. This similarity suggests a homogeneous isotopic composition of the source region and minimal influence of ancient crustal material mixing. The emplacement of mantle-derived granites in the continental crust inevitably leads to continental crustal growth (Liu et al., 2005; Tang et al., 2007; Ouxiang, 2019). However, the weakly negative εNd(t)

values and positive εHf(t) values observed in other Triassic plutons in the Beishan orogen do not imply a lack of contribution to continental crustal growth. These plutons, including the Xiaohulishan plutons, are believed to have originated from juvenile mantle-derived materials. This suggests a process of juvenile continental growth occurring in the CAOB during the Triassic, as supported by Li et al. (2012), Jahn et al. (2009, 2004), and Kovalenko et al. (2004) (Jahn et al., 2004; Kovalenko et al., 2004; Jahn et al., 2009; Li et al., 2012a). Additionally, the granites from the EQP, which formed during the transition from post-orogenic to intracontinental extensional settings, potentially signify the beginning of significant crustal growth during the Triassic, as depicted in Figure 12.

5 Conclusion

(1) Zircon U-Pb dating obtained the intrusion ages of 217.5 ± 1.3 Ma and 217.2 ± 0.8 Ma for the EQP, and 207.5 ±2 Ma for the WQP. The age of Rb mineralization can be limited to 207.5± 2.0 Ma, while the age of W-Sn-Mo mineralizations is considered to be slightly younger than approximately 217 Ma.
(2) The Rb mineralization originated from Rb-bearing parental magma that intruded upwards from the source area in the intracontinental extensional tectonic setting. During the process of intrusion, the parent magma undergoes strong differentiation, melt-fluid interaction with the enrichment of Rb, eventually forming the Rb ore body.
(3) The Qiyishan Triassic granitoids are considered to originate from the mantle-derived mafic magmas intruding into the lower crust, showing the characteristics of highly fractionated I-type granite, and characterised by a transition to A-type like granite to some extent. The magmas underwent fractional crystallization, crustal contamination and melt-fluid interaction during the subsequent upward emplacement.
(4) The granites from the East Qiyishan Pluton formed in a transitional stage in the tectonic environment, signifying the shift from post-orogenic to intracontinental extensional settings in beishan orogenic belt during late Triassic.

Data availability statement

The original contributions presented in the study are included in the article/Supplementary Material, further inquiries can be directed to the corresponding author.

Author contributions

RL: Writing–original draft. CC: Writing–review and editing. XL: Writing–review and editing. ZZ: Writing–original draft. BR: Supervision, Writing–review and editing. SZ: Funding acquisition, Writing–review and editing. EH: Project administration, Writing–review and editing.

Funding

The author(s) declare that no financial support was received for the research, authorship, and/or publication of this article.

Acknowledgments

We express our gratitude to the staff and management of the Inner Mongolia Fengyin Company for their valuable assistance during fieldwork and sample collection.

Conflict of interest

Author EH was employed by Inner Mongolia Yunfan Geological Environment Technical Service Co LTD.

The remaining authors declare that the research was conducted in the absence of any commercial or financial relationships that could be construed as a potential conflict of interest.

The reviewer FW declared a shared affiliation with the authors RL, CC, XL, ZZ, BR to the handling editor at time of review.

Publisher's note

Supplementary material

The Supplementary Material for this article can be found online at: https://www.frontiersin.org/articles/10.3389/feart.2023.1260852/full#supplementary-material

References

Baker, J., Peate, D., Waight, T., and Meyzen, C. (2004). Pb isotopic analysis of standards and samples using a 207Pb204Pb double spike and thallium to correct for mass bias with a double-focusing mcicpms. *Chem. Geol.* 211 (34), 275–303. doi:10.1016/j.chemgeo.2004.06.030

Ballouard, C., Poujol, M., Boulvais, P., Branquet, Y., Tartèse, R., and Vigneresse, J. L. (2016). Nb-Ta fractionation in peraluminous granites: A marker of the magmatic-hydrothermal transition. *Geology* 44, 231–234. doi:10.1130/g37475.1

Bau, M. (1996). Controls on the fractionation of isovalent trace elements in magmatic and aqueous systems: evidence from Y/Ho, Zr/Hf, and lanthanide tetrad effect. *Contrib. Mineral. Petrol* 123, 323–333. doi:10.1007/s004100050159

Bleousova, E. A., Grifflin, W. L., and O Reilly, S. Y. (2006). Zircon crystal morphology, trace element signatures and Hf isotope composition as a tool for petrogenetic modelling: examples from eastern Australian granitoids. *J. Petrology* 47 (2), 329353. doi:10.1093/petrology/egi077

Bouvier, A., Vervoort, J. D., and Patchett, P. J. (2008). The LuHf and SmNd isotopic composition of CHUR: constraints from unequilibrated chondrites and implications for the bulk composition of terrestrial planets. *Earth Planet. Sci. Lett.* 273 (1/2), 48–57. doi:10.1016/j.epsl.2008.06.010

Chappell, B. W., and White, A. J. R. (1992a). I and S-type granites in the Lachlan Fold Belt. *Trans. R. Soc. EdinbEarth Sci.* 83, 1–26. doi:10.1017/s0263593300007720

Chappell, B. W., and White, A. J. R. (1992b). I- and S-type granites in the Lachlan Fold Belt. *Trans. R. Soc. Edinb. Farth Sei.* 83, 1–26. doi:10.1017/s0263593300007720

Chen, B., and Arakawa, Y. (2005). Elemental and ndsr isotopic geochemistry of granitoids from thewest junggar foldbelt (nw China): with implications for phanerozoic continental growth. *Geochimica Cosmochimica Acta* 69 (5), 1307–1320. doi:10.1016/j.gca.2004.09.019

Chen, B., Jahn, B. M., and Tian, W. (2009). Evolution of the solonker suture zone: constraints from zircon U-Pb ages, Hf isotopic ratios and wholerock NdSr isotope compositions of subduction and collisionrelated magmas and forearc sediments. *J. Asian Earth Sci.* 34, 245–257. doi:10.1016/j.jseaes.2008.05.007

Chen, Z. J., Xing, G. F., Jiang, Y., et al. (2013). Paleoproterozoic type A rhyolite porphyry of the Chinese land massif Discoveries and their geological significance. *Geotect. Metallogenia* 3, 499510. doi:10.3969/j.issn.1001-552.2013.03.014

Chun, S. M., and Zhao, Q. (2004). Zircon SHRIMP ages of Guanshan amphibolite, Rizhao City, Shandong Province:Indo-Chinese magmatic thermal events and their qualification of the folding history of ultrahigh-pressure metamorphic rocks[J]. *Geol. Bull.* 23 (12), 5. doi:10.3969/j.issn.1671-2552.2004.12.015

Clemens, J. D., Holloway, J. R., and White, A. J. R. (1986). Origin of an A-type granite; experimental constraints. *American Mineralogist* 71 (3-4), 317–324. https://pubs.geoscienceworld.org/msa/ammin/article-abstract/71/3-4/317/41818/Origin-of-an-A-type-granite-experimental.

Coleman, D. S., Gray, W., and Glazner, A. F. (2004). Rethinking the emplacement and evolution of zone dplutons: geochronologic evidence for incremental assembly of the tuolumne intrusive suite, California. *Geology* 32, 433. doi:10.1130/g20220.1

CollinsW, J., Beams, S. D., White, A. J. R., and Chappell, B. W. (1982). Nature and origin of A-type granites with particular reference to south eastern Australia. *Contrib. Mineral. Petrol* 80, 189–200. doi:10.1007/bf00374895

Ding, S., Huang, H., Niu, Y. L., Zhao, Z. D., Yu, X. H., and Mo, X. X. (2011). Geochemistry, geochronology and petrogenesis of East Kunlun high NbTa rhyolites. *Acta Petrol. Sin.* 27 (12), 36033614. http://www.ysxb.ac.cn/article/id/aps_20111208.

Dumitru, T. A., and Hendrix, M. S. (2001). FissionTrack constraints on jurassic folding and thrusting in southern Mongolia and their relationship to the beishan Thrust belt of northern China. *Mem. Geol. Soc. Am.* 194, 215–229. doi:10.1130/0813711940.215

Eby, G. N. (1992). Chemical subdivision of the A-type granitoids: petrogenetic and tectonic implications. *Geology* 20 (7), 641. doi:10.1130/0091-7613(1992)020<0641:csotat>2.3.co;2

Eby, G. N. (1990). The A-type granitoids: A review of their occurrence and chemical characteristics and speculations on their petrogenesis. *Lithos* 26 (1/2), 115–134. doi:10.1016/0024-4937(90)90043-z

Fisher, C. M., Vervoort, J. D., and Hanchar, J. M. (2014). Guidelines for reporting zircon Hf isotopic data by LAMCICPMS and potential pitfalls in the interpretation of these data. *Chem. Geol.* 363, 125–133. doi:10.1016/j.chemgeo.2013.10.019

Gelman, S. E., Deering, C. D., Bachmann, O., Huber, C., and Gutiérrez, F. J. (2014). Identifying the crystal graveyards remaining after large silicic erup tions. *Earth Planet Sci. Lett.* 403, 299–306. doi:10.1016/j.epsl.2014.07.005

Gillespie, J., Glorie, S., Xiao, W. J., Zhang, Z., Collins, A. S., Evans, N., et al. (2017). Mesozoic reactivation of the beishan, southern central asian orogenic belt: insights from low temperature thermochronology. *Gondwana Res.* 43, 107–122. doi:10.1016/j.gr.2015.10.004

Gong, Q. S., Liu, M. Q., Li, H. L., Liang, M. H., and Dai, W. J. (2002). The type and basic characteristics of Beishan orogenic belt. *Gansu. Northwest. Geol.* 35, 2834. doi:10.3969/j.issn.1009-6248.2002.03.004

Gong, Q. S., Liu, M. Q., Liang, M. H., and Li, H. L. (2003). The tectonic facies and tectonic evolution of Beishan orogenic belt. *Gansu. Northwest. Geol.* 23, 1117. doi:10.3969/j.issn.1009-6248.2003.01.002

He, S. P., Ren, B. S., Yao, W. G., and Fu, L. P. (2002). The division of tectonic units of Beishan area. *GansuInner Mong. Northwest Geol.* 35, 2940. doi:10.3969/j.issn.1009-6248.2002.04.004

He, S. P., Zhou, H. W., Ren, B. C., Rao, W. G., and Fu, L. P. (2005). Crustal evolution of Palaeozoic in Beishan area, Gan su and Inner Mongolia, China. *Northwest. Geol.* 38, 615. doi:10.3969/j.issn.1009-6248.2005.03.002

He, Z. Y., Zong, K. Q., Jiang, H. Y., Xiang, H., and Zhang, Z. M. (2014). Early paleozoic tectonic evolution of the southern beishan orogenic collage: insights from the granitoids. *Acta Petrol. Sin.* 30 (8), 23242338.

Hong, D. W., Wang, S. G., Han, B. F., et al. (1995). Tectonic environment classification and identification of alkaline granite. *Sci. China (Series B)* 25 (4), 418426. doi:10.3321/j.issn:1006-9240.1995.04.001

Hsü, K. J., Yao, Y. Y., Li, J. L., and Wang, Q. C. (1992). Geology of the beishan mountains and the tectonic evolution of Northwest China. *Eclogae Geol. Helvetiae* 85, 213225. https://www.researchgate.net/publication/279594188_Geology_of_the_Beishan_Mountains_and_the_tectonic_evolution_of_Northwest_China.

Hu, Z. C., Liu, Y. S., Gao, S., Liu, W., Yang, L., Zhang, W., et al. (2012). Improved *in situ* Hf isotope ratio analysis of zircon using newly designed X skimmer cone and Jet sample cone in combination with the addition of nitrogen by laser ablation multiple collector ICPMS. *J. Anal. Atomic Spectrom.* 27, 1391. doi:10.1039/c2ja30078h

Huang, Z. B., and Jin, X. (2006). Tectonic environment of basic volcanic rocks in the Hongshishan ophiolite melange zone, Beishan Mountains, Gansu. *Geol. China* 33, 10301037. doi:10.3969/j.issn.1000-3657.2006.05.011

Jahn, B. M., Wu, F. Y., Capdevila, R., Martineau, F., Zhao, Z. H., and Wang, Y. X. (2001). Highly evolved juvenile granites with tetrad REE patterns: the woduhe and baerzhe granites from the great X ing'an mountains in NE China. *Lithos* 59 (4), 171–198. doi:10.1016/s0024-4937(01)00066-4

Jahn, B. M., Capdevila, R., Liu, D. Y., Vernon, A., and Badarch, G. (2004). Sources of phanerozoic granitoids in the transect BayanhongorUlaan baatar, Mongolia: geochemical and Nd isotopic evidence, and implications for phanerozoic crustal growth. *J. Asian Earth Sci.* 23, 629–653. doi:10.1016/s1367-9120(03)00125-1

Jahn, B. M., Litvinovsky, B. A., Zanvilevich, A. N., and Reichow, M. (2009). Peralkaline granitoid magmatism in the MongolianTransbaikalian belt: evolution, petrogenesis and tectonic significance. *Lithos* 113, 521–539. doi:10.1016/j.lithos.2009.06.015

Jahn, B. M., Wu, F. Y., and Chen, B. (2000). Granitoids of the Central Asian orogenic belt and continental growth in the Phanerozoic. *Trans. R. Soc. Edinb. Earth Sci.* 91, 181–193. doi:10.1017/s0263593300007367

Jia, X. F., Wang, Q., et al. (2009). Research progress and significance of Type A granite. *Geotect. Metallogenia* 33 (3), 465480. doi:10.3969/j.issn.1001-1552.2009.03.017

Jin, Li, han, S., Zhu., X. kun, and Pan, C. xu (2017). Production and certification of the reference material GSB 0432582015 as a 143Nd/144Nd isotope ratio reference. *Geostand. Geoanal. Res.* 41, 255262. doi:10.1111/ggr.12151

Johansson, Å., Waight, T., Andersen, T., and Simonsen, S. L. (2016). Geochemistry and petrogenesis of mesoproterozoic A-type granitoids from the Danishisland of Bornholm, southern fennoscandia. *Lithos* 244, 94–108. doi:10.1016/j.lithos.2015.11.031

Julian, A. P., Nigel, B. W., and Andrew, G. T. (1984). Trace element discrimination diagrams for the tectonic interpretation of granitic rocks. *J. Petrology* 25 (4), 956983. doi:10.1093/petrology/25.4.956

Kawabe, I. (1999). Thermochemical parameters for solution of lanthanide(III) ethylsulphate and trichloride hydrate series: tetrad effects and hydration change in aqua Ln3+ ion series. *Geochem. Jourmal* 33 (4), 249–265. doi:10.2343/geochemj.33.249

King, P. L., Chappell, B. W., Allen, C. M., and White, A. J. R. (2001). Are A-type granites the hightemperature felsic granites? Evidence from fractionated granites of the Wangrah suite. *Aust. J. Earth Sci.* 48, 501–514. doi:10.1046/j.1440-0952.2001.00881.x

Kovalenko, V. I., Yarmolyuk, V. V., Kovach, V. P., Kotov, A. B., Kozakov, I. K., Salnikova, E. B., et al. (2004). Isotopic provinces, mechanism of generation and sources of the continental curst in the central asian mobile belt: geological and isotopic evidence. *J. Asian Earth Sci.* 23, 605627. doi:10.1016/s1367-9120(03)00130-5

Li, C. F., Li, X. H., Li, Q. L., Guo, J. H., and Yang, Y. H. (2012c). Rapid and precise determination of Sr and Nd isotopic ratios in geological samples from the same filament loading by thermal ionization mass spectrometry employing a singlestep separation scheme. *Anal. Chim. Acta* 727 (10), 54–60. doi:10.1016/j.aca.2012.03.040

Li, H. Q., Chen, F. W., Li, J. Y., Qu, W. J., Wang, D. H., Wu, H., et al. (2006). Age of mineralization and hostrocks in the baishan rheniummolybdenum district, East Tianshan, Xinjiang, China: revisited. *Geol. Bull. China* 25 (8), 916922. doi:10.1109/ICOSP.2006.344496

Li, J., and Huang, X. L. (2013). Mechanism of TaNb enrichment and magmatic evolution in the yashan granites, Jiangxi province, South China. *Acta Petrol. Sin.* 29 (12), 43114322.

Li, J., Zhang, J., et al. (2009a). Crustal tectonic division and evolution of the southern part of the North Asian orogenic region and its adjacent areas. *J. Jilin Univ. (Earth Sci. Ed.* 39 (4), 584605. doi:10.3969/j.issn.1671-5888.2009.04.002

Li, M., Ren, B. F., Duan, X. L., Tian, J., Duan, L. F., and Niu, W. C. (2020). Petrogenesis of triassic granites in xiaohongshan area, beishan orogenic belt: constraints from zircon U-Pb ages and Hf isotopes. *Geol. Bull. China* 39 (9), 14221435. doi:10.3969/j.issn.1671-2552.2010.04.005

Li, N. B., Shan, Q., Zhang, Y. P., et al. (2012b). Preliminary study on A-type rhyolite porphyry in Awulaleh area, western tianshan mountains. *Geotect. Metallogenia* 36 (4), 624633. doi:10.3969/j.issn.1001-1552.2012.04.016

Li, S., Wang, T., Tong, Y., Wang, Y. B., Hong, D. W., and Ouyang, Z. X. (2011). Zircon U-Pb age, origin and its tectonic significances of Huitongshan Devonian K-feldspar granites from Beishan orogen, NW China. *Acta Petrol. Sin.* 27 (10), 30553070. doi:10.1016/j.pgeola.2011.03.006

Li, S., Wang, T., Wilde, S. A., Tong, Y., Hong, D., and Guo, Q. (2012a). Geochronology, petrogenesis and tectonic implications of Triassic granitoids from Beishan, NW. *Lithos* 134135, 123145. doi:10.1016/j.lithos.2011.12.005

Li, S., Wang, T., Tong, Y., Hong, D. W., and Ouyang, Z. X. (2009b). Identification of the early Devonian Shuangfengshan A-type granites in Liuyuan area of Beishan and its implications to tectonic evolution. *Acta Petrologica Mineralogica* 28, 407422. doi:10.1016/S1874-8651(10)60080-4

Li, X. H., Zhou, H. W., Li, Z. X., et al. (2002). Trace element and SmNd isotopic constraints on the genesis of neoproterozoic bimodal volcanic rocks in western Sichuan

and their tectonic significance. *Chin. J. Geol.* 3, 264276. doi:10.1080/12265080208422884

Liang, T., Lu, R., Yang, N., Wang, Li, and Wen, J. (2020). RbSr isochron age and isotopic compositions of H, O, S and Pb of the Gaozhuang gold deposit, Xixia county, henan province: identification of intraplate orogenic metallogenesis in northern qinling mountain. *Geol. China* 47 (2), 406425. doi:10.12029/gc20200210

Liu, M. Q., Wang, J. J., Dai, W. J., and Dang, Y. Y. (2005). Genesis and geological significance of positive εNd(t) granitoids in the Hongshishan area in the Beishan orogenic belt, Gansu China. *Geol. Bull. China* 24 (9), 831–836. doi:10.3969/j.issn.1671-2552.2005.09.008

Liu, M. Q., Wang, J. J., Dai, W. J., and Dang, Y. Y. (2006). The U-Pb age of singlegrained zircon from Maanshanbei granite in Hongshishan area of the Beishan orogenic belt Gansu Province. *Acta Petrologica Mineralogica*, 473479. doi:10.3969/j.issn.1000-6524.2006.06.003

Liu, X. Y., and Wang, Q. (1995). Tectonics and evolution of the Beishan orogenic belt, West China. *Geol. Res.* 10, 151165. http://cpfd.cnki.com.cn/Article/CPFDTOTAL-ZGDJ199500001007.htm.

Liu, Y. S., Gao, S., Hu, Z. C., Gao, C. G., Zong, K. Q., and Wang, D. B. (2010). Continental and oceanic crust recyclinginduced meltperidotite interactions in the TransNorth China orogen: U-Pb dating, Hf isotopes and trace elements in zircons of mantle xenoliths. *J. Petrology* 51 (12), 537571. doi:10.1093/petrology/egp082

Ludwig, K. R. (2003). *Isoplot 3.00: a geochronological Toolkit for Microsoft excel*. Berkeley, CA, USA: Berkeley Geochronology Center California, 39.

Ludwig, K. R. (1998). On the treatment of concordant uraniumlead ages. *Geochimica Cosmochimica Acta* 62 (4), 665–676. doi:10.1016/s0016-7037(98)00059-3

Lv, B., Yang, Y. Q., Meng, X. G., et al. (2011). Geochemical characteristics and genesis of alkali-feldspar granite in Dongqiyishan, Inner Mongolia. *Acta Petrologica Mineralogica* 30 (03), 543552. doi:10.3969/j.issn.1000-6524.2011.03.017

Maniar, P. D., and Piccoli, P. M. (1989). Tectonic discrimination of granitoids. *Geol. Soc. Am. Bull.* 101 (5), 635–643. doi:10.1130/0016-7606(1989)101<0635:tdog>2.3.co;2

Mao, Q. G. (2008). *Paleozoic to early Mesozoic accretionary and collisional tectonics of the Beishan and adjacent area, Northwest China: Beijing, China, Chinese Academy of Sciences*. Ph. D. Thesis. Institute of Geology and Geophysics, 228.

Mao, Q. G., Xiao, W. J., Han, C. M., Sun, M., Yuan, C., Zhang, J. E., et al. (2009). Discovery of middle silurian adakite granite and its tectonic significance in liuyuan area, beishan Moutains, NW China. *Acta Petrol. Sin.* 26, 584896. http://www.ysxb.ac.cn/article/id/aps_20100219.

Mao, Q., Xiao, W., Fang, T., Wang, J., Han, C., Sun, M., et al. (2011). Late ordovician to early devonian adakites and nbenriched basalts in the liuyuan area, beishan, NW China: implications for early paleozoic slabmelting and crustal growth in the southern Altaids. *Gondwana Res.* 22, 534–553. doi:10.1016/j.gr.2011.06.006

Miao, Q. (2018). *Characteristics and mineralization of the Madialkali feldspar granite in eastern Hebei province*. Beijing, China: China University of Geosciences.

Middlemost, E. A. K. (1994). Naming materials in the magma/igneous rock system. *Earth Sci. Rev.* 37 (34), 215–224. doi:10.1016/0012-8252(94)90029-9

Miller, C. F., and Mittlefehldt, D. W. (1984). Extreme fractionation in felsic magma chambers: A product of liquidstate diffusion or fractional crystallization? *Earth Planet Sci. Lett.* 68, 151–158. doi:10.1016/0012-821x(84)90147-x

Miller, C. F., and Mittlefehldt, D. W. (1982). Depletion of light rareearth elements in felsicmagmas. *Geology* 10, 129. doi:10.1130/0091-7613(1982)10<129:dolrei>2.0.co;2

Mushkin, A. (2003). The petrogenesis of A-type magmas from the AmramMassif, southern Israel. *J. Petrology* 44 (5), 815–832. doi:10.1093/petrology/44.5.815

Nie, F. J., Jiang, S. H., Bai, D. M., Wang, X. L., Su, X. X., Li, J. C., et al. (2002c). "Metallogenic studies and ore prospecting in the conjunction area of Inner Mongolia Autonomous Region," in *Gansu province and Xinjiang Uygur autonomous region (beishan Mt.), northwest China: beijing* (Beijing, China: Geological Publishing House), 408.

Nie, F. J., Jiang, S. H., Liu, Y., et al. (2002a). SmNd isotope age of fluorite and its geological significance in Qiyishan large fluorite deposit. *East Alxa Mineral. Deposits* 1 (1), 1015. doi:10.3969/j.issn.0258-7106.2002.01.002

Nie, F. J., Jiang, S. H., Liu, Y., Chen, W., Liu, X. Y., and Zhang, S. H. (2002b). 40Ar/39Ar Isotopic age dating on K-feldspar separates from eastern Huaniushan granite, Gansu province, and its geological significance. *Chin. J. Geol.* 37, 415422.

Ouxiang, W. (2019). *Research on the genesis of Xiaohulishan molybdenum polymetallic deposit in eastern TianshanBeishan area*. Anhui, China: Hefei University of Technology. doi:10.27101/d.cnki.ghfgu

Peccerillo, A., and Taylor, A. R. (1976). Geochemistry of Eocene calc-alkaline volcanic rocks from the Kastamonu area, Northern Turkey. *Contributions Mineralogy Petrology* 58 (1), 63–81. doi:10.1007/bf00384745

Peng, H., Wang, J., Liu, C., Zhang, S., Niu, Y., Zhang, T., et al. (2023). Mesozoic tectonothermal evolution of the southern central asian orogenic belt: evidence from apatite fissiontrack thermochronology in Shalazha Mountain, inner Mongolia. *J. Earth Sci.* 34 (1), 37–53. doi:10.1007/s12583-020-1053-z

Peng, Z., Li, H., Zhang, S., Xu, M., Yan, C., and Cai, M. (2010). Geochemical characteristics of Mo mineralized granite in the Xiaohulishan deposite, Inner Mongolia. *Geol. Explor.* 46 (02), 291298. doi:10.3724/SP.J.1231.2010.06586

Pérez-Soba, C., and Villaseca, C. (2010). Petrogenesis of highly fractionated I-type peraluminous granites: La Pedriza pluton (Spanish Central System)[J]. *Geol. Acta* 8 (2). doi:10.1344/105.000001527

Petford, N. (2003). Rheology of granitic magmas during ascent and emplacement. *Annu. Rev. Earth PlanetSci* 31, 399–427. doi:10.1146/annurev.earth.31.100901.141352

PetfordN, C. A. R., McCaffrey, K. J. W., and Vigneresse, J. L. (2000). Granite magma formation, transport and emplacement in the Earth'scrust. *Nature* 408, 669–673. doi:10.1038/35047000

Pitcher, W. S. (1997). *The natureand origin of granite*. 2nd ed, Boca Raton, Fl, USA: Chapman & Hall, 387.

Qiu, L., Yan, D. P., Zhou, M. F., Arndt, N. T., Tang, S. L., and Qi, L. (2014). Geochronology and geochemistry of the late triassic longtan pluton in SouthSouth China: termination of the crustal melting and indosinian orogenesis. *Int. J. Earth Sci. Geol. Rundsch)* 103, 649–666. doi:10.1007/s005310130996z

Şengör, A. M. C., Natal'in, B. A., and Burtman, U. S. (1993). Evolution of the Altaid tectonic collage and Paleozoic crustal growth in Eurasia. *Nature* 364, 209304. https://www.nature.com/articles/364299a0.

Shi, G. Z., Liang, C., Wang, H., and Huang, C. (2019). Superimposed deformation of the solonker belt and nearby regions in western inner Mongolia, China. *Geol. Mag.* 156 (5), 811–832. doi:10.1017/S0016756818000183

Song, C. N., Li, H., He, L., et al. (2002). Polygonal criterion for data processing of U-Pb discordant ages of grain-scale zircons determined by thermal ion mass spectrometry--an example of deep metamorphic rocks in the Dabie Mountains and the East Kunlun Mountains. *Geol. Sci. Technol. Inf.* (03), 24–29. doi:10.3969/j.issn.1000-7849.2002.03.00

Song, D. F., Song, D., Xiao, W. J., Xiao, W., Han, C. M., Han, C., et al. (2013). Geochronological and geochemical study of gneiss–schist complexes and associated granitoids, Beishan Orogen, southern Altaids. *Int. Geol. Rev.* 55 (14), 1705–1727. doi:10.1080/00206814.2013.792515

Song, D. F., Xiao, W. J., Han, C. M., Tian, Z. H., and Li, Y. C. (2018). Accretionary processes of the central segment of beishan: constraints from structural deformation and 40ar39ar geochronology. *Acta Petrol. Sin.* 34 (7), 20872098.

Stepanov, A., Mavrogenes, A., Meffre, S., and Davidson, P. (2014). The key role of mica during igneous concentration of tantalum. *Contrib. Mineral. Petrol* 167, 1009. doi:10.1007/s00410-014-1009-3

Su, B. X., Qin, K. Z., Sakyi, P. A., Liu, P. P., Tang, D. M., Malaviarachchi, S. P. K., et al. (2011). Geochemistry and geochronology of acidic rocks in the beishan region, NW China: petrogenesis and tectonic implications. *J. Asian Earth Sci.* 41, 31–43. doi:10.1016/j.jseaes.2010.12.002

Sun, S. S., and McDonough, W. F. (1989). Chemical and isotopic systematics of oceanic basalts; implications for mantle composition and processes. *Geol. Soc. Spec. Publ.* 42, 313–345. doi:10.1144/gsl.sp.1989.042.01.19

Sylvester, P. J. (1989). Postcollisional alkaline granites. *J. Geol.* 97, 261–280. doi:10.1086/629302

Tang, J. H., Gu, L. X., Zhang, Z. Z., Wu, C. Z., San, J. Z., Wang, C. S., et al. (2007). Characteristics, age and origin of the Xianshuiquan gneissose granite in eastern Tianshan. *Acta Petrol. Sin.* 23 (8), 18031820. doi:10.1631/jzus.2007.B0900

Tian, Z. H., Xiao, W. J., Sun, J. M., Windley, B. F., Glen, R., Han, C. M., et al. (2015). Triassic deformation of permian early Triassic arcarc-related sediments in theBeishan (NW China): last pulse of the accretionary orogenesis in the southernmost Altaids. *Tectonophysics* 662, 363–384. doi:10.1016/j.tecto.2015.01.009

Tian, Z. H., Xiao, W. J., Windley, B. F., Lin, L. N., Han, C. M., Zhang, J. E., et al. (2014). Structure, age, and tectonic development of the Huoshishan–Niujuanzi ophiolitic mélange, Beishan, southernmost Altaids. *Beishan, S. Altaids Gondwana Res.* 25 (2), 820–841. doi:10.1016/j.gr.2013.05.006

Tian, Z. H., Xiao, W. J., Zhang, Z. Y., and Lin, X. (2016). FissonTrack Constrains on superposed folding in the beishan orogenic belt, southernmost Altaids. *Geosci. Front.* 7 (2), 181–196. doi:10.1016/j.gsf.2015.11.007

Vermeesch, P. (2018). IsoplotR: A free and open toolbox for geochronology. *Geosci. Front.* 9, 1479–1493. doi:10.1016/j.gsf.2018.04.001

Wang, H. L., Xu, X. Y., He, H. P., and Chen, J. L. (2007). *Geological map of the Chinese tian Shan and its adjacent areas, 1:1,000,000*. Beijing, China: Geological Publishing House.

Wang, S. D., Zhang, K. C., FenningWang, J. S., BowenLi, J. W., WenDai, P., et al. (2021). Recognition of a Permian to Triassic foreland basin in the central Beishan Orogen, NW China: provenance variations and their constraints on latest Palaeozoic orogeny. *Palaeogeogr. Palaeoclimatol. Palaeoecol. Int. J. GeoSciences* 565 (1), 110168. doi:10.1016/j.palaeo.2020.110168

Wang, Y., Lu, Q., Meng, G., et al. (2009). Alkali feldspathic granite and its mineralization in East Qiyishan, inner Mongolia. *Acta Geol. Sin.* 83 (10), 1505–1514. doi:10.3321/j.issn:0001-5717.2009.10.015

Wang, Y., Li, J. Y., and Sun, G. H. (2008b). Post collisional eastward extrusion and tectonic exhumation along the eastern tianshan orogen, central Asia: constraints from dextral strikeslip motion and 40Ar/39Ar geochronological evidence. *J. Geol.* 116, 599–618. doi:10.1086/591993

Wang, Y., Sun, G., and Li, J. (2010). U-Pb (SHRIMP) and 40Ar/39Ar geochronological constraints on the evolution of the Xingxingxia shear zone, NW

China: A triassic segment of the Altyn Tagh fault system. *Geol. Soc. Am. Bull.* 122, 487–505. doi:10.1130/b26347.1

Wei, B., Wang, C. Y., Zhao, Z., and Bao, H. (2020). Columbite-group minerals and mica of peraluminous granite record the magmatic-hydrothermal processes that formed the Zhaojinggou Ta Nb deposit in the North China Craton. *Lithos* 370-371 (4), 105648. doi:10.1016/j.lithos.2020.105648

Wei, Z. J., Huang, Z. B., Sun, Y. J., and Huo, J. C. (2004). Geological characteristics of ophiolite migmatitic complex of Hongshishan region. *Gansu. Northwest Geol.* 37, 1318. doi:10.3969/j.issn.1009-6248.2004.02.003

Whalen, J. B., Currie, K. L., and Chappell, B. W. (1987). A-Type granites: geochemical characteristics,discrimination and petrogenesis. *Contributions Mineralogy Petrology* 95 (4), 407–419. doi:10.1007/bf00402202

Wu, C. Z., Jia, L., Lei, R. X., Chen, B. Y., Feng, Z. J., Feng, Y. G., et al. (2021a). Advances and general characteristics of the amazonite granite and related rubidium deposits in Central Asian Orogenic Belt. *Acta Petrol. Sin.* 37 (9), 2604–2628. doi:10.18654/10000569/2021.09.02

Wu, C. Z., Jia, L., Lei, R. X., Chen, B. Y., Feng, Z. J., Feng, Y. G., et al. (2021b). Advances and general characteristics of the amazonite granite and related rubidium deposits in Central Asian Orogenic Belt. *Acta Petrol. Sin.* 37 (9), 2604–2628. doi:10.18654/1000-0569/2021.09.02

Wu, F. Y., Liu, X. C., Ji, W. Q., Wang, J. M., and Yang, L. (2017a). Highly fractionated granites: recognition and research. *Sci. China Earth Sci.* 60, 1201–1219. doi:10.1007/s1143001651391

Wu, F. Y., Sun, D. Y., Li, H. M., Jahn, B. m., and Wilde, S. (2002). A-Type granites in northeastern China: age and geochemical constraints on their petrogenesis. *Chem. Geol.* 187 (1), 143–173. doi:10.1016/s0009-2541(02)00018-9

Wu, F. Y., Guo, C. L., Hu, F. Y., Liu, X. C., Zhao, J. X., Li, X. F., et al. (2023). Petrogenesis of the highly fractionated granites and their mineralizations in Nanling Range, South China. *Acta Petrol. Sin.* 39 (1), 1–36. doi:10.18654/1000.0569/2023.01.01

Wu, F. Y., Li, X. H., Yang, J. H., and Zheng, Y. F. (2007a). Discussions on the petrogenesis of granites. *Acta Petrol. Sin.* 23 (6), 1217–1238. doi:10.3969/j.issn.1000-0569.2007.06.001

Wu, F. Y., Li, X. H., Zheng, Y. F., and Gao, S. (2007b). LuHf isotopic systematics and their applications in petrology. *Acta Petrol.* 23 (2), 185220. doi:10.1016/j.sedgeo.2006.03.028

Wu, F. Y., Liu, X. C., Liu, Z. C., Wang, R. C., Xie, L., Wang, J. M., et al. (2020). Highly fractionated Himalayan leucogranites and associated rare -metal mineralization. *Lithos* 352-353, 105319. doi:10.1016/j.lithos.2019.105319

Wu, Y. S., Chen, Y. J., and Zhou, K. F. (2017b). Mo deposits in Northwest China: geology geochemistry geochronology and tectonic setting. *Ore Geol. Rev.* 81, 641–671. doi:10.1016/j.oregeorev.2016.07.010

WuZhang, H. H. Z., Wang, T., Guo, L., Zhang, Y., et al. (2020). Geochronology, geochemistry, mineralogy and metallogenic implications of the Zhaojinggou Nb-Ta deposit in the northern margin of the North China Craton, China. *Ore Geol. Rev.* 125, 103692. doi:10.1016/j.oregeorev.2020.103692

Xiao, W. J., Huang, B. C., Han, C. M., Sun, S., and Li, J. L. (2010b). A review of the western part of the Altaids: A key to understanding the architecture of accretionary orogens. *Gondwana Res.* 18, 253–273. doi:10.1016/j.gr.2010.01.007

Xiao, W. J., Mao, Q. G., Windley, B. F., Han, C. M., Qu, J. F., Zhang, J. E., et al. (2010a). Paleozoic multiple accretionary and collisional processes of the Beishan orogenic collage. *Am. J. Sci.* 310, 1553–1594. doi:10.2475/10.2010.12

Xiao, W. J., Windley, B. F., Huang, B. C., Han, C. M., Yuan, C., Chen, H. L., et al. (2009). EndPermian to midTriassic termination of the accretionary processes of the southern Altaids: implications for the geodynamic evolution, phanerozoic continental growth, and metallogeny of central Asia. *Int. J. Earth Sci.* 98, 1189–1217. doi:10.1007/s00531-008-0407-z

Xiao, W. J., Zhang, L. C., Qin, K. Z., Sun, S., and Li, J. L. (2004). Paleozoic accretionary and collisional tectonics of the eastern tianshan (China): implications for the continental growth of central Asia. *Am. J. Sci.* 304, 370395. doi:10.2475/ajs.304.4.370

Yang, H. Q., Zhao, G. B., Li, Y., Jiang, H. B., Tan, W. J., Ren, H. N., et al. (2012). The relationship between Paleozoic tectonic setting and mineralization in XinjiangGansuInner Mongolia juncture area. *Geol. Bull. China* 31 (2/3), 413421. doi:10.3969/j.issn.1671-2552.2012.02.027

Yang, J. H., Wu, F. Y., Chung, S. L., Wilde, S. A., and Chu, M. F. (2006). A hybrid origin for the Qian-Shan A-type granite, northeast China: geochemical and SrNdHf isotopic evidence. *Lithos* 89 (1), 89–106. doi:10.1016/j.lithos.2005.10.002

Yang, Y., Lu, Bo, Meng, G., et al. (2013). Geochemistry of granites from East Qiyi Mountain, Inner Mongolia, zircon SHRIMPU-Pb ages and the environment of rock formation. *Earth J.* (2), 13. doi:10.3975/cagsb.2013.02.04

Yuan, S., and Zhao, P. (2021). New synthetic fluid inclusion method to investigate partition behavior of ore metals between melt and fluid phases (in Chinese). *Sci. Sin. Terrae* 51 (2), 241–249. doi:10.1360/SSTe-2020-013.1

Zhang, W., and Hu, Z. (2020b). Spectroscopy A. Estimation of isotopic reference values for pure materials and geological reference materials. *At. Spectrosc.* 41 (3), 93102. doi:10.46770/AS.2020.03.001

Zhang, W., Hu, Z. C., and Liu, Y. S. (2020a). IsoCompass: new freeware software for isotopic data reduction of LAMCICPMS. *J. Anal. At. Spectrom.* 35, 1087–1096. doi:10.1039/d0ja00084a

Zhang, W., Jian, P., Liu, D. Y., and Hou, K. J. (2010a). Geochemistry, geochronology and Hf isotopic compositions of Triassic granodioritediorite and shoshonite from the Damaoqi area, central Inner Mongolia, China. *Geol. Bull. China* 29, 821832. doi:10.3969/j.issn.1671-2552.2010.06.004

Zhang, W., Wu, T. R., he, Y. K., Feng, J. C., and Zheng, R. G. (2010). LAICPMS zircon U-Pb ages of Xijianquanzi alkalirich potassiumhigh granites in Beishan, Gansu province,and their tectonic significance. *Acta Petrologica Mineralogica* 29, 719731. doi:10.1016/S1002-0160(11)60127-6

Zhang, X. H., Liu, J. H., Xu, J. L., Niu, H. B., and Zhao, Y. Q. (2005a). Second study on the plate tectonics in Gansu Province. *Acta Geol. Gansu* 14, 110.

Zhang, X. H. (1993). Tectonostratigraphic evolution of the qilian and beishan orogenic belt in Gansu, Qinghai, inner Mongolia. *Acta Geol. Gansu* 2, 8086. http://www.cnki.com.cn/Article/CJFDTotal-GSDZ199301009.htm.

Zhang, Y. L., Xu, R. K., Shan, L., Jia, Q. Z., Song, Z. B., Chen, X. Y., et al. (2012b). Rockforming and ore-forming ages of the Xiaohulishan molybdenum deposit in Beishan area, Inner Mongolia. *Geol. Bull. China* 31 (2/3), 469475. doi:10.1007/s11783-011-0280-z

Zhang, Y. Y., Dostal, J., Zhao, Z. H., Liu, C., and Guo, Z. J. (2011). Geochronology, geochemistry and petrogenesis of mafic and ultramafic rocks from southern beishan area, NW China: implications for crustmantle interaction. *Gondwana Res.* 20, 816–830. doi:10.1016/j.gr.2011.03.008

Zhang, Z. Z., Gu, L. X., Wu, C. Z., Li, W. Q., Xi, A. H., and Wang, S. (2005b). Zircon SHRIMP dating for the Weiya pluton, eastern tianshan: its geological implications. *Acta Geol. Sin. Engl. Ed.* 79, 481490. doi:10.1111/j.1755-6724.2005.tb00914.x

Zhao, K. D., Jiang, S. Y., Sun, T., et al. (2006). "Hf-Nd isotopic decoupling of Indochinese granites in the western part of the South Ridge and petrogenetic implications," in *National Symposium on Petrology and geodynamics* (Jiangsu, China: Nanjing University).

Zhao, P. L., Zajacz, Z., Tsay, A., Chu, X., Cheng, Q. M., and Yuan, S. D. (2022). The partitioning behavior of Mo during magmatic fluid exsolution and its implications for Mo mineralization. *Geochimica Cosmochimica Acta* 339, 115–126. doi:10.1016/j.gca.2022.10.020

Zhao, Y. Q., Liu, M. Q., Zhang, W. R., and Dai, W. J. (2003). Discovery of early paleozoic ordovician strata in the hongshishan area, beishan mountains, Gansu, China. *Geol. Bull. China* 22 (3), 215.

Zhao, Z. F., Zheng, Y. F., Li, S. G., et al. (2005). "Oisotopic equilibrium in the Shuanghe ultrahigh pressure metamorphic minerals of the Dabie Mountains and its constraints on the validity of SmNd and RbSr isochrones ages," in *Chinese society of mineral and rock geochemistry* (Beijing, China: Geological Society of China), 4.

Zhao, Z. H., Guo, Z. J., and Wang, Y. (2007). Geochronology, geochemical characteristics and tectonic implications of the granitoids from Liuyuan area, Beishan, Gansu province, northwest China. *Acta Petrol. Sin.* 23, 18471860.

Zheng, Y. F., and Chen, R. X. (2021). Extreme metamorphism and metamorphic facies series at convergent plate boundaries: implications for supercontinent dynamics. *Geosphere* 17, 1647–1685. doi:10.1130/ges02334.1

Zheng, Y. F., and Chen, R. X. (2017). Regional metamorphism at extreme conditions: implications for orogeny at convergent plate margins. *J. Asian Earth Sci.* 145, 46–73. doi:10.1016/j.jseaes.2017.03.009

Zheng, Y. F., Chen, Y. X., Chen, R. X., and Dai, L. Q. (2022). Tectonic evolution of convergent plate margins and its geological effects. *Sci. China EarthSciences* 65 (7), 1247–1276. doi:10.1007/s1143002299476

Zheng, Y. F. (2023). Plate tectonics in the twentyfirst century. *Sci. China Earth Sci.* 66 (1), 1–40. doi:10.1007/s1143002210119

Zhou, T. F., Yuan, F., Zhang, D. Y., Fan, Y., Liu, s, Peng, M. X., et al. (2010). Geochronology, mineralization of granitoids in Jueluotage area, eastern Tianshan, Xinjiang. *Acta Petrol. Sin.* 26. http://www.ysxb.ac.cn/article/id/aps_20100212.

Zong, K. Q., Klemd, R., Yuan, Y., He, Z. Y., Guo, J. L., Shi, X. L., et al. (2017). The assembly of Rodinia: the correlation of early neoproterozoic (ca. 900 ma) highgrade metamorphism and continental arc formation in the southern beishan orogen, southern central asian orogenic belt (CAOB). *Precambrian Res.* 290, 32–48. doi:10.1016/j.precamres.2016.12.010

Zuo, G. C., and He, G. Q. (1990a). *Plate tectonics and metallogenic regularities in beishan region*. Beijing, China: Peking University Publishing House Beijing, 226.

Zuo, G. C., Liu, Y. K., and Liu, C. Y. (2003). Framework and evolution of the tectonic structure in beishan area across Gansu province, Xinjiang autonomous region and inner Mongolia autonomous region. *Acta Geol. Gansu* 12, 115.

Zuo, G. C., Zhang, S. L., He, G. Q., and Zhang, Y. (1991). Plate tectonic characteristics during the early Paleozoic in Beishan near the SinoMongolian border region, China. *Tectonophysics* 188, 385–392. doi:10.1016/0040-1951(91)90466-6

Zuo, G. C., Zhang, S. L., Wang, X., Jin, S. Q., He, G. Q., Zhang, Y., et al. (1990b). *Plate tectonics and metallogenic regularities in Beishan region*. Beijing, China: Peking University Publishing House, 226.